JOURNAL OF BIOMOLECULAR STRUCTURE AND DYNAMICS
https://doi.org/10.1080/07391102.2020.1837679

Secondary metabolites from spice and herbs as potential multitarget inhibitors of SARS-CoV-2 proteins

Saurabh Gupta[a], Vishal Singh[b], Pritish Kumar Varadwaj[b], Navajeet Chakravartty[a], A. V. S. Krishna Mohan Katta[a], Sivarama Prasad Lekkala[a], George Thomas[c], Srinivasan Narasimhan[d], Arjula R. Reddy[e] and V. B. Reddy Lachagari[a]

[a]AgriGenome Labs Pvt. Ltd., Hyderabad, India;[b]Department of Applied Sciences, Indian Institute of Information Technology, Allahabad, India; [c]AgriGenome Labs Pvt. Ltd., Kakkanad, India; [d]Asthagiri Herbal Research Foundation, Chennai, India; [e]Department of Plant Sciences, University of Hyderabad, Hyderabad, India

Communicated by Ramaswamy H. Sarma

ABSTRACT

Severe acute respiratory syndrome coronavirus 2 (SARS-CoV-2) has been responsible for the current global pandemic that has caused a death toll of >1.12 million worldwide and number continues to climb in several countries. Currently, there are neither specific antiviral drugs nor vaccines for the treatment and prevention of COVID-19. We screened *in silico*, a group of natural spice and herbal secondary metabolites (SMs) for their inhibition efficacy against multiple target proteins of SARS-CoV-2 as well as the human angiotensin-converting enzyme 2 protein. Docking and simulation results indicated that epicatechin, embelin, hesperidin, cafestol, murrayanine and murrayaquinone-A have higher inhibition efficacy over at least one of the known antiviral drugs such as Hydroxychloroquine, Remdesivir and Ribavirin. Combination of these potentially effective SMs from their respective plant sources was analysed, and its absorption and acute oral toxicity were examined in Wistar rats and classified as category 5 as per the Globally Harmonized System. The identified SMs may be useful in the development of preventive nutraceuticals, food supplements and antiviral drugs.

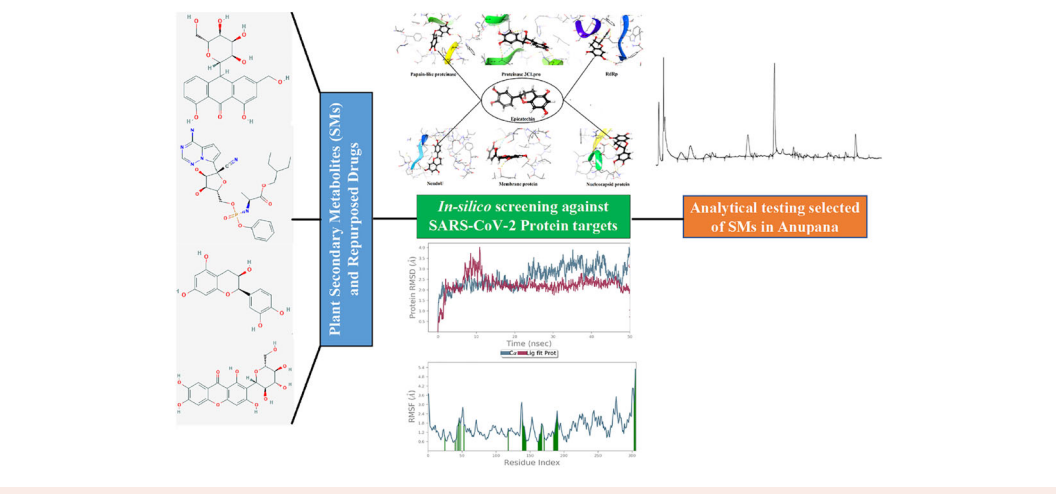

Abbreviations: COVID-19: coronavirus disease 2019; E: envelope protein; ER: endoplasmic reticulum; ExoN: Guanine-N7 methyltransferase; DMV: double-membrane vesicle; hACE2: human angiotensin-converting enzyme 2; Hel: helicase; HPLC: high-performance liquid chromatography; LC-MS: liquid chromatography–mass spectrometry; M: membrane protein; MD: molecular dynamics; MERS-CoV: Middle East respiratory syndrome coronavirus; NC: nucleocapsid protein; NendoU: nidoviral RNA uridylate-specific endoribonuclease; Nsp: non-structural protein; RBD: receptor binding domain; RCT: replicase/transcriptase complex; S: spike glycoprotein; SARS-CoV-2: severe acute respiratory syndrome coronavirus 2; SM: secondary metabolite

ARTICLE HISTORY
Received 3 August 2020
Accepted 11 October 2020

KEYWORDS
Anupama; SARS-CoV-2; epicatechin; hesperidin; murrayanine; docking and simulation

CONTACT V. B. Reddy Lachagari vb.reddy@aggenome.com; Saurabh Gupta saurabh.g@aggenome.com AgriGenome Labs Pvt. Ltd., SINC, IKP Knowledge Park Genome Valley, Shamirpet, Hyderabad, Telangana 500 101, India.

Supplemental data for this article can be accessed online at https://doi.org/10.1080/07391102.2020.1837679

Highlights

- Secondary metabolites (SMs) from selected spices and herbs were screened *in silico* for their interactions with SARS-CoV-2 proteins.
- Epicatechin and hesperidin emerged as potent multitarget inhibitors with better inhibition efficacy *in silico* in comparison with some of the known antiviral drugs.
- Anupana, a herbal extract was shown to contain epicatechin, hesperidin and mangiferin.
- It is suggested that the data presented here may be useful in development of preventive nutraceuticals, food supplements and antiviral drugs.

Introduction

Severe acute respiratory syndrome coronavirus 2 (SARS-CoV-2) is responsible for the current global pandemic of coronavirus disease 2019 (COVID-19) that began in Wuhan, Hubei province of China (Huang et al., 2020; Wang, Xu, et al., 2020; Zhu et al., 2020). It belongs to *Coronaviridae* family of Nidovirales order and has the characteristic crown-like spikes on its outer surface. Members of the *Coronaviridae* family such as SARS-CoV (Drosten et al., 2003; Ge et al., 2013; Ksiazek et al., 2003; Wang et al., 2005), Middle-East respiratory syndrome coronavirus (MERS-CoV) (Zaki et al., 2012), and SARS-CoV-2 have crossed the species barrier to cause deadly pneumonia in humans since the beginning of the 21st century (Guan et al., 2020). SARS-CoV-2 has infected more than 40.4 million peoples across the world and caused more than 1.12 million deaths as on October 21, 2020 as per World Health Organization. Highly pathogenic zoonotic pathogens SARS-CoV, MERS-CoV, and SARS-CoV-2 belong to the β-coronavirus genus and low-pathogenicity coronaviruses *Viz.* HCoV-OC43, HCoV-HKU1, HCoV-NL63, and HCoV-229E belong to α-coronavirus genus and they cause infections in humans (Owusu et al., 2014).

In December 2019, SARS-CoV-2 was isolated and in January 2020, the 29,800 bp long single-strand RNA genome sequence was reported (Zhou et al., 2020; Zhu et al., 2020). As on October 21, 2020 there are 92 genomes assembled and annotated, and 29,569 genome sequences deposited in NCBI from across the world (https://www.ncbi.nlm.nih.gov/sars-cov-2/). Although only a few variants have been observed among the sequenced genomes so far, a high level of homology and conserved genome architecture is clearly observed among them. Transmembrane spike glycoprotein (S) protruding from the viral surface of SARS-CoV-2 is reported to form homotrimers with human angiotensin-converting enzyme 2 (hACE2) receptor to enter target cells (Kirchdoerfer et al., 2018; Song et al., 2018). The receptor binding domain (RBD) region of S glycoprotein is recognized by the critical lysine 31 residue of the hACE2 receptor protein (Wan et al., 2020). Conformational change occurs in S protein once it is bound to the receptor and this facilitates viral envelope infusion into the cell membrane via endosomal pathway. Subsequently, SARS-CoV-2 uses the host ribosome to release the RNA genome having 5′-untranslated region (5′-UTR), open reading frames *orf1a/b* (longest), 3, 6, 7a, 7b, 8, 9b as well as spike, envelope, membrane, nucleocapsid proteins, and 3′-untranslated region (3′-UTR). The *orf1a* encodes 16 Non-structural proteins (Nsps) which form the replicase/transcriptase complex (RTC), while the remaining *orfs* produce structural and accessory proteins (Shereen et al., 2020; Wu, Liu, et al., 2020; Zhou et al., 2020). The RNA and viral proteins assemble into virions in the endoplasmic reticulum (ER) and Golgi and are then transported by vesicles to the cell membrane to be released out of the cell.

Nsp 1 and 2 inhibit and modulate host translation mechanism while Nsp 3 and 5 act as proteases that cleave and activate the viral polyprotein. Nsp7 forms a hexadecamer with Nsp8 and may participate in viral replication by acting as a primase. RNA-directed RNA polymerase (RdRp) complex is formed by Nsp 7, 8, and 12 and participate in replication and transcription, whereas Helicase (Hel/Nsp13) and Guanine-N7 methyltransferase (ExoN/Nsp14) are responsible for unwinding and proofreading, respectively. Nsp10/Nsp16 complex plays a pivotal role in viral transcription by stimulating ExoN and 2-*O*-MT activity. Uridylate-specific endoribonuclease (NendoU) is associated with RNA processing that include RNA endonuclease activity producing 2′-3′ cyclic phosphodiester and 5′-hydroxyl termini activity (Kim et al., 2020; Romano et al., 2020). The structural proteins i.e. S, membrane protein (M), nucleocapsid protein (NC) and envelope protein (E) are responsible for virus morphogenesis and assembly. Further, Nsp 4 and 6 participate in vesicle formation and induction of autophagosomes from the host ER. Of these viral proteins, Papain-like proteinase (Nsp3), Proteinase 3CLpro (Nsp5), RdRp, S and NC proteins have been the candidates of choice as potential drug targets (Sanders, 2020). However, no new drug that specifically interacts with SARS-CoV-2 proteins has been developed yet, though some repurposed drugs are being currently employed.

Alternate medicines, mostly herbal and spice based have now assumed importance in countries like India and several such preparations are already in the market. Spices and medicinal plants are essential ingredients in the traditional Indian cuisinewhich are known to be rich in a wide range of biologically active secondary metabolites (SMs). For long, extracts containing these SMs have been used as antiviral, anti-inflammatory, anticancer agents as well as a cure for diabetes in the Indian traditional herbal medicine practice known as "Ayurveda." For instance, one such Ayurvedic concoction, Anupana, is a combination of herbal ingredients, taken along with food and medicine for improving their absorption and bioavailability (Jaseela & Krishna, 2019). Most of these herbal formulations are based on traditional wisdom and from ancient medical treatises. Some of the SMs were shown to have empirically defined pharmacological properties (Ang et al., 2020; Sachan et al., 2018; Wu, Zhao, et al., 2020; Zachariah & Leela, 2018) and are taken routinely as a simple component of food or as health supplements based on specific indications. The advantage being that in most cases, they have no major side-effects. However, not much is known about the precise molecular mechanisms by which SMs interact with various structural and functional molecules impacting vital viral processes such as absorption, replication,

host transcription and translation, host suppression, pathogenesis and spread. Advances in metabolomics, genomics, and bioinformatics provide powerful tools to investigate the scientific basis for such properties exhibited by these herbs, spices, and other plant extracts. In the present work, we have investigated the molecular interaction between selected SMs from well-known herbs and spices, and the target proteins of the virus involved in well characterised functions. We analysed their potential inhibitory activity against all the encoded SARS-CoV-2 proteins. Our study reveals that six of these SMs are superior in their inhibitory activity over some of the well-known and or repurposed antiviral drugs in the market. In addition, we present *in silico* and biochemical data showing that the herbal concoction, Anupana, contains three of these SMs *viz.* epicatechin, hesperidin and mangiferin that are shown to be highly active as inhibitors of viral proteins, thus providing a reasonable basis for further clinical investigation.

Materials and methods

Target proteins of SARS-CoV-2

The genome of SARS-CoV-2 is known to produce a total of 27 proteins. Of these, 17 are selected as potential target proteins for screening of naturally available SMs from various herbs and spices. Among these, crystal structures have been recently released for eight proteins *viz*. Papain-like proteinase, Proteinase 3CLpro, Nsp7-Nsp8 complex, Nsp9, Nsp10-Nsp16 complex, RdRp, NendoU, S and NC. Nsp1, Nsp2, Nsp4, Nsp6, Hel, ExoN, M and E; they have been modelled using Swiss Model (https://swissmodel.expasy.org/) and I-Tasser web server (https://zhanglab.ccmb.med.umich.edu/). Additionally, we have also selected human hACE2 enzyme as the target protein to study its possible interaction with these SMs. The details about these proteins, their function, binding sites, grid size and hydrogen bonding residues are listed in Table 1.

Selection of SMs from Indian medicinal and spices plants

Based on literature and traditional knowledge, we selected SMs that were reported to have anti-inflammatory, anti-cancer and/or anti-viral activities and their details are given in Table S1. Along with these SMs, we also selected known drugs, *viz.* Arbidol (Umifenovir), Chloroquine, Colchicine, Dexamethasone, Hydroxychloroquine, Losartan, Remdesivir, Ribavirin, Oseltamivir and Quinazoline, some of these are currently being used for the treatment COVID-19. ADMET for each compound were calculated using Qikprop tool of the Schrodinger suite (QikProp; Schrödinger, LLC, New York, NY, 2020).

Docking and molecular dynamics simulation

Protein preparation wizard program was used to prepare, *in silico* and each selected protein and a grid was prepared on the binding site of each protein (Table 1). The ligand preparation was performed for all selected compounds (Table S1) using LigPrep (Epik; Schrödinger, LLC). Single-precision (SP) glide docking algorithm that has good scoring function for receptor-ligand interaction was used to perform docking. SP uses a number of hierarchical filters to identify the possible interacting locations of the ligand in the binding-site of the receptor protein. The shape and properties of the receptor binding site are represented by the grid and their coordinates are listed in Table 1. The compounds were ranked based on the docking score (Glide; Schrödinger, LLC). The program also calculates different scores such as ligand efficacy, H-bond, lipo, evdw, etc. Two-dimensional interaction diagrams for top protein-ligand complexes were generated. Based on docking score, ligand efficacy, and H-bond interaction analysis, best complex was selected for molecular dynamics (MD) simulation and performed using OPLS 2005 force field in Desmond molecular dynamics package incorporated in Schrodinger suite (Bowers et al., 2006). Selected protein-ligand complexes were solvated in TIP4P water model in an orthorhombic box with periodic boundary conditions. For each system, charges were neutralized using appropriate cation (Na^+) or anion (Cl^-) along with a salt concentration of 0.15 mol/L. The prepared system was energy minimized for a convergence threshold of 1.0 kcal/mol/Å by using the steepest descent method, and the NPT ensemble was used for minimization and relaxation of the system. 300° K standard temperature and 1.013 bar pressure level was maintained during production run of 50 ns. The generated MD trajectories were analysed and RMSD, RMSF and Hydrogen bond interactions were calculated for each using in-built trajectory analysis tool for Desmond (Maestro-Desmond Interoperability Tools; Schrödinger, LLC).

Testing and validation of Anupana constituents

Docking and simulation studies reveal that active molecules against SARS-CoV-2 are SM and belong to ketone, polyphenol, carbazole, tannin and flavonoid families. This prompted us to develop and evaluate Anupana described in Ayurveda. Accordingly, we analysed the extract on high-performance liquid chromatography (HPLC) for simultaneous determination of polyphenols and flavonoids by the adopting the reported method by Sakakibara et al. (2003). Further, the Anupana formulation was analysed by Liquid Chromatography–Mass Spectrometry (LC-MS) to identify the chemicals present (Covey et al., 1986). Acute oral toxicity of this Anupana was tested on Wistar rats as per OECD Guideline No. 423, December 2001.

Results

Structural information and docking analysis of selected SM and drugs

A set of 69 plant SMs were selected based on the antiviral properties indicated merely by traditional knowledge and lacking in rigorous scientific evidence of their underlying molecular interactions with the virus (Table S1). Molecular

Table 1. List of selected protein targets of SARS-Cov2 and human ACE2 receptor with their functions, grid size and binding sites for docking analysis.

No.	Protein name	Sequence length	Structure information and PDB ID	Protein functions	Grid centre, inner and outer box size in X, Y, Z dimension	Binding site residues*	References
1	Host translation inhibitor (Nsp1)	180	3D structure is modelled using chain A of 2HSX	Inhibits INF signalling and blocks the host translation via interacting with the 40S ribosomal subunit. This leads to suppression of host gene expression and facilitates efficient viral gene expression in infected cells and blocks innate immune response.	52.99 × 60.07 × 52.94, 20 × 20 × 20 and 50 × 50 × 50	Val35, **Glu36**, Val38, Leu39, Glu41, Ala42, His45, Pro67, Tyr68, **Leu88**, **Ala90**, **Glu91**, **Thr151**, **Asp152**, **Glu155**	Almeida et al., 2007; Jauregui et al., 2013; Shen et al., 2019
2	Non-structural protein 2 (Nsp2)	638	3D structure is modelled using chain A of 2HSX	Plays a role in the modulation of host cell survival signalling pathway via interacting with host prohibitin protein i.e. PHB and PHB2. These two proteins play an important role in maintaining the functional integrity of the mitochondria and protecting cells from various stresses.	70.794 × 35.812 × 2.181, 10 × 10 × 10 and 30 × 30 × 30	Lys142, Cys143, Cys146, Cys161, **Glu167**, **Tyr242**, **Agr246**, Ser248, Ile251, Cys253, **His255**, **Val258** Leu270, Leu271, Ile296, Phe300, Leu314, Gln321, Ser325	Angeletti et al., 2020
3	Papain-like proteinase (Nsp3)	1945	Crystal structure of Papain-like protease domain (6W9C)	Responsible for the cleavages located at the N-terminus of the replicase polyprotein. Promotes cytokine expression and cleavage of viral polyprotein.	−39.02 × 13.21 × 37.13, 20 × 20 × 20 and 50 × 50 × 50	Lys105, **Trp106**, **Asp108**, Lys157, **Leu162**, Asp164, **Glu167**, Tyr264 **Asn267**, Tyr268 **Gln269**, Cys270, Gly271	Angeletti et al., 2020
4	Non-structural protein 4 (Nsp4)	500	3D structure is modelled using chain A of 3VCB	Participates in the assembly of virally induced cytoplasmic double-membrane vesicles necessary for viral replication.	1.12 × 1.89 × 56.68, 20 × 20 × 20 and 50 × 50 × 50	**Asn174**, **Glu177**, Arg190, Val192, Gly196, Asp217, Ser229, **Arg228**, **Asp259**, **Agr400**, Leu421, **Asn423**, **Lys424**, Glu425, **Gly482**, Ser483, Val485, **Leu486**	Sakai et al., 2017
5	Proteinase 3CLpro (Nsp5)	306	Selected crystal structure of Proteinase 3CLpro 6LU7	Cleaves the C-terminus of replicase polyprotein at 11 sites. Recognizes substrates containing the core sequence [ILMVF]-Q-|-[SGACN]. Also, able to bind an ADP-ribose-1′′-phosphate (ADRP). Promoting cytokine expression and cleavage of viral polyprotein	78.97 × 69.56 × 75.28., 20 × 20 × 20 and 50 × 50 × 50	Thr24, Thr25, Thr26, Leu27, His41, **Phe140**, Leu141, Asn142, **Gly143**, Ser144, **Cys145**, His163, **His164**, Met165, **Glu166**, Pro168, His172, **Arg188**, **Gln189**, **Thr190**, Ala191, Gln192	Anand et al., 2003
6	Non-structural protein 6 (Nsp6)	290	3D structure is modelled using chain A of 4AV3	Plays a role in the initial induction of autophagosomes from host reticulum endoplasmic. Later, limits the expansion of these phagosomes that are no longer able to deliver viral components to lysosomes. Contribute to structure of DMVs as transmembrane scaffold protein (DMVs formation)	47.18 × 53.77 × 47.05, 20 × 20 × 20 and 50 × 50 × 50	Thr172, **Ser173**, **Thr180**, Tyr219, **Phe225**, **Gly226**, leu230, Met 254, **Asn255** Gly258, **Leu259**, **Asn264**, Ser265, **Ile266**, **Asp267**, Ala268, Phe269	Benvenuto et al., 2020

(*continued*)

Table 1. Continued.

No.	Protein name	Sequence length	Structure information and PDB ID	Protein functions	Grid centre, inner and outer box size in X, Y, Z dimension	Binding site residues*	References
7	Nsp7-Nsp8 complex protein	Nsp7:83; Nsp8:198	Selected crystal structure of Nsp7 and the C-terminal domain of Nsp8 complex 6WQD	Nsp7 forms hexadecamer with Nsp8 and may participate in viral replication by acting as a primase. Alternatively, may synthesize substantially longer products than oligonucleotide primers. Processivity clamp for RNA polymerase by arms hexadecameric complex	5.56 × −1.57 × 16.26, 20 × 20 × 20 and 50 × 50 × 50	Asp101, Ans104, Asn105, **Asn108**, **Asp112**, **Asn140**, Thr141, Thr148, **Ser151**, Ala152, leu153	Astuti and Ysrafil, 2020; Te Velthuis et al., 2012
8	Non-structural protein 9 (Nsp9)	113	Selected crystal of Nsp9 RNA binding protein 6W4B	RNA binding protein phosphatase and functions as ssRNA-binding protein during viral replication.	52.86 × 56.1 × 51.46, 20 × 20 × 20 and 40 × 40 × 40	Ala43, Tyr89, Phe90, Arg99, Gly100, Met101, Val102, **Leu103**, Gly104, Ser105, **Ala107**, **Val110**, **Leu112**	Littler et al., 2020; Sutton et al., 2004
9	Nsp10-Nsp16 complex protein	Nsp10:139; Nsp16:298	Selected crystal structure of Nsp10-Nsp16 complex 6W75	Has a pivotal role in viral transcription by stimulating ExoN and 2-*O*-MT activity (viral mRNAs cap methylation).	85.84 × 15.68 × −0.96, 20 × 20 × 20 and 50 × 50 × 50	**Asn6841**, **Lys6844**, Tyr6845, **Gly6871**, Ser6872, Asp6873, Asp6897, Leu6898, Asp6912, **Cys6913**, Met6929, **Asp6928**, **Asp6931**, **Lys6968**	Decroly et al., 2011
10	RNA-directed RNA polymerase (RdRp)	932	Selected crystal structure of RdRp protein 6M71	Responsible for replication and transcription	114.58 × 115.26 × 122.09, 10 × 10 × 10 and 30 × 30 × 30	Arg555, Val557, Asn611, Trp617 **Asp618**, Tyr619, **Lys621** Asp623, Thr680 Ser682, Ser682, Asn691, Phe753, Ser754 **Ser759**, **Asp760**, **Asp761**, **Lys798**, **Trp800**, **Ser814**	Dong et al., 2020; Dutta et al., 2020; Gao et al., 2020; Romano et al., 2020
11	Helicase (Hel)	601	3D structure is modelled using chain B of 5WWP	Has a metal-binding domain in N-terminus, displaying RNA and DNA duplex-unwinding activities with 5′ to 3′ polarity	94.07 × 98.04 × 108.29, 30 × 30 × 30 and 66 × 66 × 66	**Arg178**, Asn179, **Glu197**, Glu261, Phe262, Pro284, Gly285, Thr286, Gly287, Lys288, Ser289, His290, Phe291, **Arg339**, **Met378**, **Asn361**, **Asp383** Gln404, Ala407, Thr410, **Leu412**, Thr416, **Leu417**, Arg442, Arg443, **Asp534**, Glu540, Asn557, **Arg560**, Arg567	Hao et al., 2017; Jia et al., 2019
12	Guanine-N7 methyl transferase (ExoN)	527	3D structure is modelled using chain B of 5C8S	Enzyme possesses two different activities: an exoribonuclease activity acting on both ssRNA and dsRNA in a 3′ to 5′ direction and a N7-guanine methyltransferase activity.	63.31 × 55.57 × 61.23, 20 × 20 × 20 and 50 × 50 × 50	Trp292, Gly333, Pro335, **Asp352**, Ala353, **Gln354**, Leu366, Phe367, **Tyr368**, Trp385, **Asn386**, Cys387, Val389, **Asn422**, **His424**, Phe426, **His427**	Ferron et al., 2018; Ma et al., 2015
13	Nidoviral RNA uridylate-specific endoribo-nuclease (NendoU)	346	Selected crystal structure 6VWW	Associated with RNA processing, has an RNA endonuclease activity producing 2′-3′ cyclic phosphodiester and 5′-hydroxyl termini.	−91.92 × 20.15 × −30.79, 10 × 10 × 10 and 30 × 30 x30	**His235**, **Asp240**, Gly247, **Gly248** His250, Lys290, **Ser294**, **Glu340**, Thr341, **Tyr343**, Pro344	Kim et al., 2020; Romano et al., 2020

(*continued*)

Table 1. Continued.

No.	Protein name	Sequence length	Structure information and PDB ID	Protein functions	Grid centre, inner and outer box size in X, Y, Z dimension	Binding site residues*	References
14	Spike glycol-protein (S)	1273	Selected crystal structure of spike glycoprotein of SARS-Cov-2 6VYB (Open state)	Spike protein (open state) attaches the virion to the cell membrane by interacting with host receptor, initiating the infection. The receptor binding domain (RBD) of this protein bind to human ACE2 and CLEC4M/DC-SIGNR receptors and internalization of the virus into the endosomes of the host cell induces conformational changes in the S glycoprotein (close state).	201.99 × 189.28 × 256.27, 10 × 10 × 10 and 30 × 30 × 30	RBD found between 449 to 510 residues, binding site residues are: **Gly404**, Lys417, **Tyr453**, **Thr495**, Gly496, Phe497, **Asn501**, Gly504, Tyr505	Ou et al., 2020; Walls et al., 2020
15	Membrane protein (M)	222	3D structure is modelled using chain A of 3W6Q	Component of the viral envelope that plays a central role in virus morphogenesis and assembly via its interactions with other viral proteins.	56.1 × 52.77 × 54.37, 20 × 20 × 20 and 50 × 50 × 50	Leu34, Arg42, Phe45, Lys50, Leu51, Leu54, Ile97, Leu102, Arg105, Arg107, Pro123, **Glu135**	Bianchi et al., 2020
16	Nucleo-capsid protein (NC)	419	Selected crystal structure NC protein 6M3M	The second largest surface protein of virus that involved in packaging of positive strand of viral genome RNA into a helical ribonucleocapsid (RNP). Plays a fundamental role during virion assembly through its interactions with M protein and the viral genome.	12.22 × −8.87 × −13.09, 20 × 20 × 20 and 50 × 50 × 50	**Thr55**, **Ala56**, Arg88, Arg89, Thr91, Agr92, **Tyr110**, Tyr112, Thr115	Kang et al., 2020
17	Envelope protein (E)	75	3D structure is modelled using chain A of 2ZJA	Integral membrane protein that involved in several aspects of the virus' life cycle, such as assembly, envelope formation, budding, and pathogenesis. In host membranes it forms pentameric protein-lipid pores that allow ion transport. Also plays a role in the induction of apoptosis. Activates the host NLRP3 inflammasome, leading to IL-1beta overproduction.	46.07 × 46.66 × 42.61, 20 × 20 × 20 and 50 × 50 × 50	**Leu 19**, Val24, Phe26, Leu27, Leu28, Leu31, Ala32, Ile33, Thr35, Ala36, **Asn45**, **Asp48**, **Lys53**, **Asp72**	Schoeman and Fielding, 2019, Bianchi et al., 2020
18	hACE2 protein		Selected chain A of crystal structure of hACE2 protein 6M0J	The host receptor in humans that interacts with the spike glycoprotein of the virus, binding to which makes a conformation transition that enables infusion of the virus into the host cell.	−27.41 × 16.48 × −39.03, 20, 20 × 20 and 50 × 50 × 50	Gln24, Thr27, Asp30, Lys31, His34, Glu35, Glu37, Asp38, Tyr41, Gln42, Leu79, Met82, **Gln102**, **Asp206**, Asn330, Lys353, **Asp350**, Asp355, Arg357, **Asp382**, **Tyr385**, **Leu391**, Arg393, **Glu398**, **Ala484**, **Lys562**	Chowdhury and Maranas, 2020

*Bold highlighted residues of catalytic site forming Hydrogen bonds with inhibitors.

interaction between catalytic sites of selected protein targets of SARS-CoV-2 (Table 1) with 69 plant SMs and 10 known drugs has been analysed. IUPAC name, two-dimensional structure, sources, and function of selected SMs and known drugs are listed (Table S1). We also calculated the ADMET for all selected SMs and known drugs (Table S2). The different docking scores for each protein are listed in Table S3. The details of interaction analysis of these molecules with each protein is described below.

SMs and Nsp1 interaction

Nsp1 also known as eukaryotic translation inhibitor, suppresses the host translation initiation mechanism via binding to the 40S-rRNA that leads to inhibition of host mRNA translation (Jauregui et al., 2013; Lokugamage et al., 2012; Shen et al., 2019). Modelled 3D structure of Nsp1 consists of two α-helices and six mixed parallel/antiparallel strand β-sheets with a catalytic binding residue i.e. Val35, Glu36, Val38, Leu39, Glu41, Ala42, His45, Pro67, Tyr68, Leu88, Ala90, Glu91, Thr151, Asp152, Glu155. Top five molecules based on glide-docking, ligand efficacy and h-bond scores indicate that Ribavirin (−5.84), Hydroxychloroquine (−5.134) and plant metabolites hesperidin (−5.769), embelin-2 (−5.555) and 1-phenylethanethiol (−5.128) are the best inhibitors of Nsp1. Hesperidin forms hydrogen bonds with Glu36, Ala90, Thr151 and Asp152 and embelin-2 only with Ala90. Ribavirin and Hydroxychloroquine form H-bonds with Leu88, Glu155 and Glu36, Glu91 respectively (Figure S1). Hesperidin and embelin-2 show better inhibition capability than Hydroxychloroquine.1-phenylethanethiol indicated similar ligand inhibition pattern as of Ribavirin based on docking, ligand efficacy, and H-bond score.

Nsp2 inhibition by SMs

Nsp2 is reported to modulate host cell survival signalling pathway by interacting with the host prohibitin protein of virus. Crystal structure of the protein is not reported in PDB till date. Beat homology model of Nsp2 using chain A of (2HSX) and the structure binding cavity consists of Cys161, Cys164, Glu167, Tyr242, Agr246, Ser248, Ile251, Cys253, His255, Val258 Leu270, Leu271, Ile296 and Phe300 residues (Angeletti et al., 2020). Docking results indicate that Arbidol (−7.279) shows most prominent inhibition property. 1-phenylethanethiol (−5.178) has better inhibition efficacy than artemisinin (−5.174), (−) beta Pinene (−4.584) and (−) alpha Pinene (−4.572) (Figure S2). These results indicate that 1-phenylethanethiol, a major constituent of curry leaf (*Bergera koenigii*) spice, is found to be a potent inhibitor of Nsp2.

Papain like protease inhibition by Epicatechin

Nsp3 is the longest (1,945 aa) protein among all the expressed proteins of SARS-CoV-2 genome. This protein consists of two main functional domains i.e. ADP ribose phosphatase (6W6Y) and papain-like protease domain (6W9C). This protein binds to viral RNA, nucleocapsid protein (NC) and participates in polyprotein processing (Angeletti et al., 2020). We have selected papain-like protease functional domain crystal structure for docking analysis. The protein has Zn^{2+} metal binding catalytic site (Zn^{2+} forms bond with Cys270) and a grid was generated keeping metal ion in the centre, which includes Lys105, Trp106, Asp108, Lys157, Leu162, Asp164, Glu167, Tyr264, Asn267, Tyr268, Gln269, Cys270, and Gly271 residues in the ligand binding sites. Docking results indicate that among the top five inhibitors, epicatechin (−7.469) shows best inhibition efficacy scores among selected inhibitors followed by Colchicine (−6.771), cafestol (−6.705), embelin-4 (−6.31) and artemisinin (−6.134). Epicatechin forms H-bonds with Trp106, Asp108, Glu167, Asn267 and has glide H-bond score of −0.627. However, cafestol forms H-bond with Asn267 and has glide H-bond score of −0.608. Embelin-4 forms H-bonds with Asp108, Glu167 residues. Colchicine and artemisinin form one H-bond each respectively with Leu167 and Asp108 (Figure S3). These results indicate that epicatechin, a common SM found in apple, cocoa, tea, grapes, blackberry, is a potent inhibitor of Papain like protease.

Hesperidin inhibits Nsp4

Nsp4 is known to involve in the formation of double-membrane vesicles (DMVs) structure and is a transmembrane scaffold protein necessary for viral replication. It can be a potential antiviral target in the treatment of SARS-CoV-2 infection (Sakai et al., 2017). 3D model of Nsp4 was generated and found its binding cavity includes Asn174, Glu177, Arg190, Val192, Gly196, Asp217, Ser229, Arg228, Asp259, Agr400, Leu421, Asn423, Lys424, Glu425, Gly482, Ser483, Val485, Leu486 residues. Hesperidin (−6.822) and withanolide-N (−6.716) were found to have better inhibition efficacy than Oseltamivir (−6.54) and Hydroxychloroquine (−6.303) while epicatechin (−6.288) shows similar inhibition efficacy as Hydroxychloroquine. Hesperidin forms six H-bonds with Arg228, Agr400, Asn423, Lys424, Gly482, and Leu486 residues. Withanolide-N and epicatechin form H-bonds respectively with Glu177, Glu227 and Asn174, Glu177, Lys429. Oseltamivir and Hydroxychloroquine form H-bonds with Glu177, Glu425 and Glu227, respectively (Figure S4). These results indicate hesperidin is a potent inhibitor of Nsp4, available in citrus and mint.

Proteinase 3CLpro and Epicatechin interaction leads to inhibition

Main proteinase 3CLpro is an attractive target for therapy of COVID-19 disease and has been studied by various groups. We have selected recently generated crystal structure of the main proteinase 3CLpro (6LU7) of SARS-CoV-2. Docking was performed in the known ligand binding sites and epicatechin (−6.204), embelin-4 (−6.098), curcumin (−5.981) and aloin (−5.808) have better inhibition efficacy than Ribavirin (−5.627) based on docking score. Epicatechin and embelin-4 form three H-bonds with Glu166, Arg188, Gln189 and Gln107, Phe181, Gly183, respectively (Figure S5). Aloin and curcumin form H-bonds with Phe140, Gly143, Gln189 and Phe140, Thr190. Ribavirin forms four H-bonds with Leu141,

Gly143, Arg188 and Gln189 but its ligand efficiency inside the cavity is lower than others. Epicatechin seems to have better inhibition of Proteinase 3CLpro than the other selected SMs.

Epicatechin inhibition of Nsp6 is comparable to that of Ribavirin

Nsp6 plays a role in the initial induction of autophagosomes from host ER and is also involved in the formation of DMVs (Benvenuto et al., 2020). Protein modelling of Nsp6 was performed using chain A of 4AV3 as a template. Docking results indicate that Ribavirin (−6.018), epicatechin (−5.695), embelin-4 (−5.489), embelin-3 (−5.425) and embelin-5 (−4.993) are positioned as top five inhibitors for Nsp6 protein. The interaction pattern of Ribavirin and epicatechin shows that it is forming four H-bonds with Phe225, Gly226, Asn255, Asp267 and Ser173, Gly226, Gly258 Asp267 respectively (Figure S6). Overall, comparative docking analysis indicates that natural SM epicatechin may have similar inhibition capacity as of Ribavirin for Nsp6.

Epicatechin is a potent inhibitor of Nsp7/Nsp8 complex

Nsp7 forms hexadecamer with Nsp8 and participates in viral replication by acting as a primase in RTC along with RdRp (Astuti & Ysrafil, 2020). From the crystal structure of Nsp7/Nsp8 complex (6WQD) (Kim et al., 2020), the substrate binding is found to include Asp101, Ans104, Asn105, Asn108, Asp112, Asn140, Thr141, Thr148, Ser151, Ala152, and Leu153 residues. Docking results indicate embelin (−4.678), epicatechin (−4.492), Remdesivir (−4.369), Ribavirin (−4.368) and Quinazoline (−4.207) are the top five inhibitors. Embelin and epicatechin have lower docking and ligand efficacy score while embelin lacks evidence of H-bonding in the cavity. Epicatechin and Remdesivir form three H-bonds with Asn108, Asp112, Ser151 and Asn105, Asp112, Asn140, respectively. Epicatechin seems to have similar ligand efficacy as Remdesivir (Figure S7). Overall docking results indicate that naturally available epicatechin is a potent inhibitor of Nsp6/Nsp7 complex.

Cabozole, Murrayaquinone-A and Epicatechin are inhibitory to Nsp9

Nsp9 was found to be important for replication during infection of human cells due to its oligonucleotide-binding property that plays a key role in promoting viral replication process. The RNA binding mechanism of Nsp9 protein (6W4B) family is not clearly understood, however a conserved peptide/RNA binding domain is observed (Littler et al., 2020). We have selected this conserved domain which has Gly100, Met101, Val102, Leu103, Gly104 and Ser105 as binding site residues for the molecular interaction analysis. Analysis shows that carbazole (−6.869), murrayaquinone-A (−6.754), epicatechin (−5.705), Hydroxychloroquine (−5.588) and embelin-4 (−5.467) are the top five inhibitors of Nsp9 protein. Molecular interactions indicate that Epicatechin forms three H-bonds with Leu103, Ala107, Leu112 in which Leu103 is responsible for RNA binding property of Nsp9. carbazole, murrayaquinone-A and Hydroxychloroquine form H-bond with Val110 while embelin-4 forms H-bond with Ala107 (Figure S8). Results show that cabozole and murrayaquinone-A, both abundant in curry leaves, and epicatechin showed better inhibition efficacy than hydroxychloroquine for Nsp9.

Mangiferin, Murrayanine and Epicatechin found to be inhibitory to Nsp10/Nsp16 complex

Nsp10-Nsp16 complex protein plays a pivotal role in viral transcription by stimulating exonuclease (ExoN) and viral mRNAs cap methylation activity (2-O-MT) (Decroly et al., 2011). Crystal structure of Nsp10-Nsp16 complex (6W75) from SARS-CoV2 was recently submitted to PDB. Docking analysis shows that no selected drug has been positioned in the top five inhibitors list, while SM such as hesperidin (−8.170), mangiferin (−7.529), embelin (−7.355), murrayanine (−7.254) and epicatechin (−7.237) are in top five. Hydroxychloroquine was the only drug molecule in the top ten inhibitors of this protein with docking score of −6.376. Hesperidin shows highest ligand efficacy (−1.716) forming eight H-bonds with Asn6841, Lys6844, Asp6897, Gly6871, Cys6913, Asp6928, Asp6931 and Lys6968, while mangiferin, forms five H-bonds with Gly6871, Asp6897, Asp6928, and Tyr6930 residues of catalytic site of Nsp10-Nsp16 complex (Figure S9). Overall, mangiferin and murrayanine are identified as potential inhibitor of Nsp10-Nsp16 complex besides hesperidin.

Epicatechin is a potential inhibitor of viral RdRp

RdRp complex has Nsp7, Nsp8 and Nsp12 proteins and it is the main enzyme of SARS-CoV-2 responsible for replication and transcription. The crystal structure of RdRp complex (6M71) was selected for docking and the catalytic site lies between 611 to 626 and 753 to 767 residues with the defined ligand binding residues being Asp618, Ser759, Asp760 and Asp761. Docking results indicate that among the top five potential inhibitors for RdRp, epicatechin (−5.972) showed better inhibition efficacy than Hydroxychloroquine (−5.583), aloin (−5.547) and hesperidin (−5.301) has better inhibition efficacy than Ribavirin (−5.257). In our study, Remdesivir (−4.97) got 8th rank in terms of inhibition efficacy of RdRp while five SMs are found to be better inhibitor. Molecular interaction of epicatechin shows that it forms five H-bonds (highest among all selected) with Asp760, Asp761, Lys798, Trp800 and Ser814 while Hydroxychloroquine forms three H-bonds and two electrostatics bonds with Asp760, Asp761. Similarly, aloin, hesperidin form five H-bonds with Tyr619, Asp760, Asp761, Lys798, Trp800, Glu811 and Lys551, Lys621, Asp760, Lys798, Trp800, Glu811 respectively, whereas, Ribavirin forms four H-bonds with Tyr619, Asp760, Asp761, Ser814 (Figure S10). Overall, these results show that epicatechin is a potential inhibitor of RdRp among the selected SM molecules.

Hesperidin is a potential inhibitor of viral Hel and ExoN

Hel or Nsp13 structure is modelled using crystal structure of Nsp13 (5WWP) from MERS-CoV (Hao et al., 2017). The docking scores of SMs hesperidin (−7.132), embelin − 5 (−6.444), aloin (−6.305), epicatechin (−6.265) and embelin (−5.817) show that they are the top five potential inhibitors while azadirachtin figured sixth (−5.784). Hesperidin forms five H-bonds with Arg178, Leu412, Leu417, Asp534, and Arg560. Embelin-5 forms three H-bonds with Asn361, Asp383 and Met378 and aloin forms four H-bonds with Glu142, Arg178, Arg339 and Asn361. Epicatechin forms five H-bonds with Lys139, Glu197, Thr231, Arg339, Asn361. On the other hand, azadirachtin forms only two H-bonds with Thr180 and Pro408 (Figure S11). These results indicate that hesperidin has better binding efficacy than other selected SM molecules for Helicase.

The ExoN enzyme possesses two different activities and has been modelled using chain B of crystal structure of Nsp14-Nsp10 complex (5C8S) of SARS-CoV (Ma et al., 2015). Docking studies show that hesperidin (−8.358), epicatechin (−7.746), cafestol (−7.091), withanolide-A (−6.967) and 3-HDH-Withanolide-F (−6.662) are the top five compounds that are capable of inhibiting Guanine-N7 methyltransferase and Exoribonuclease activity. Hesperidin and epicatechin form H-bonds with Asp352, Gln354, His424 and Asp352, Gln354, Asn422 respectively, whereas cafestol and withanolide-A form H-bonds with Tyr368, His427 and Asp352 Asn368 (Figure S12). These results indicate that hesperidin is the best potential inhibitor of ExoN among the selected SMs; significantly, none of the drugs tested figured in the top five positions.

Epicatechin is a potential inhibitor of NendoU

NendoU enzyme (6VWW) has endonuclease activity and is associated with this virus's RNA processing. Recently, it has been proposed that NendoU is also responsible interference with the innate immune response. This enzyme has 346 residues (39 kDa monomeric unit) folds into three domains: N-terminal, middle domain and C-terminal catalytic NendoU domain. We have selected the active site of this enzyme located in a shallow groove between the two beta-sheets and carries six key residues i.e. His235, His250, Lys290, Ser294, Thr341, Tyr343 conserved among SARS-CoV2, SARS-CoV and MERS-CoV proteins for docking analysis (Kim et al., 2020). Results indicate that epicatechin (−5.849), Ribavirin (−5.831), Remdesivir (−5.774), Losartan (−5.606) and hesperidin (−5.553) are the top five inhibitors among all selected compounds. Epicatechin forms H-bond with Ser294 whereas the drugs Ribavirin, Remdesivir and Losartan form it with Gly248, Ser294, Thr341; Lys 290, Ser294; and Ser294, respectively. Hesperidin forms H-bonds with Ser204, His235, Asp240, Gly248, Ser294 and Glu340 residues and shows comparable ligand binding efficacy (−1.166) and H-bond score (−0.042) to Remdesivir (Figure S13). Overall, these results show epicatechin has better inhibition capability than Ribavirin, Remdesivir and Losartan, while hesperidin efficacy is similar to that of Remdesivir.

Carbazole and its derivatives as a inhibitor of S

S (6VYB) is the main structural protein that enables virus to make entry into the host cell through binding to ACE2 receptor present in the membrane. The receptor binding domain (RBD) of S is located between 449 to 510 residues that interact with the host cell ACE2 receptor (Walls et al., 2020). Here, our aim was to find potential SMs that can create interference in interaction of RBD with ACE2 receptor. Recently published crystal structure of S from SARS-CoV2 (Ou et al., 2020) was used for the docking analysis employing RBD as an active site. Results indicate that carbazole (−5.113), murrayaquinone-A (−4.696), Ribavirin (−4.545), Remdesivir (−4.506) and murrayanine (−4.502) are the top five inhibitors of S protein. Molecular interaction analysis indicates that carbozol and murrayaquinone-A form one H-bond with Gly404 and Tyr453 respectively, while Ribavirin forms four with Asp405, Gln409, Lys417, Tyr453 and Remdesivir two with Gln409, Lys417 (Figure S14). Interaction analysis revealed that murrayaquinone-A can inhibit the RBD domain function via forming H-bond with Tyr453 residues and also it shows good ligand efficacy. It is noteworthy that murrayaquinone-A and murrayanine are naturally available in curry leaf which is widely used as spice in Indian cuisine.

Epicatechin as a potential inhibitor of M, NC, and E

M is the second important structural component involved in the assembly of virus particles. Molecular interaction analysis of protein and ligands show that all selected metabolites and drugs are interacting in the binding cavity of M protein. Results indicate that epicatechin (−6.462) and Remdesivir (−6.221) showed better inhibition than maurrayaquinone-A (−5.975), Losartan (−5.437) and murrayanine (−5.367) among the top five inhibitors of M protein. Molecular interaction plot indicates that Epicatechin forms three H-bonds with Thr9, Thr130, Thr135 while Remdesivir forms two with Trp20 and His125. Murrayaquinone-A forms H-bond with Tyr9 and Losartan forms it with His125 of the catalytic site of M protein (Figure S15). These results show that epicatechin is the best inhibitor of M protein among all the tested SMs.

NC (6M3M) is involved in packaging of positive strand of viral genome RNA into a helical ribonucleocapsid (RNP). The N-terminal RNA binding domain cavity includes Thr55, Ala56, Gly61, Arg88, Arg89, Thr91, Agr92, Tyr110 and Tyr112 residues, which are known to interact with RNA to form RNP. Blocking of this domain may lead to virion assembly disruption and reduce the viral replication (Kang et al., 2020). Docking analysis shows that epicatechin (−5.538), embelin (−5.12), carbazole (−4.883), Hydroxychloroquine (−4.828) and 1-phenylethanethiol (−4.705) are the top five potential inhibitors of NC protein. epicatechin and embelin form H-bonds with Arg90, Glu119, Asp129 and Arg90, Asp129 respectively, while Hydroxychloroquine forms three with Gln59, Gly61 and Asp64 (Figure S16). These results indicate that epicatechin is the best inhibitor of NC among the screened SMs.

E is the smallest integral part of the membrane proteins involved in the packaging of viral RNA. It has three main domains i.e., short hydrophilic N-terminal domain (7–12 amino acids), hydrophobic transmembrane domain (25 aa

long), and long hydrophilic C-terminal domain (8–10 aa). Docking of selected inhibitors in the identified cavity of the modelled E protein shows that carbazole (−4.885), Remdesivir (−4.561), murrayanine (−4.496), Ribavirin (−4.484), Losartan (−4.35) are among the top five inhibitors, whereas murrayaquinone-A (−4.339), Epicatechin (−4.316) also showed good inhibition. Molecular interaction between binding site and ligands indicates that residues Asn45, Asp48, Lys53 form three H-bonds with Remdesivir, Ribavirin and epicatechin, while carbazole, murrayanine, murrayaquinone-A H-bond with Leu19, Asp72, Asp72, respectively (Figure S17). Epicatechin has similar interaction patterns as of Remdesivir and Ribavirin with higher glide H-bond scores showing that it can be a potent inhibitor of E protein.

Hesperidin as blocker of virus entry via interacting with human ACE2

Human ACE2 is the host receptor that interacts with the spike glycoprotein of the virus, binding to which makes a conformation transition that enables infusion of the virus into the host cell (Chowdhury & Maranas, 2020). From the ACE2 protein (Chain A) crystal structure (6M0J), spike receptor-binding residues of hACE2 *viz.* Gln24, Thr27, Asp30, Lys31, His34, Glu35, Glu37, Asp38, Tyr41, Gln42, Leu79, Met82, Asn330, Lys353, Asp350, Asp355, Arg357, Asp382, Tyr385, Arg393, Glu398, Lys562 were selected as binding cavity and a grid was generated. Docking analysis shows hesperidin (−8.111), epicatechin (−6.603), embelin-5 (−6.551), Hydroxychloroquine (−6.096), Hyoscyamine (−5.993) and aloin (−5.859) to be the top inhibitors for hACE2. Hesperidin and epicatechin form H-bonds with Gln102, Asp350, Asp382, Tyr385, Leu391, Ala484, Lys562 and Asp206, Glu398, Lys562, respectively. Hydroxychloroquine forms H-bonds with Asp350, Tyr385, Phe390 and electrostatic bond with Asp350 while aloin also forms H-bonds with Asp350, Asp382, Phe390 Asn394 with better inhibition than Hyoscyamine (Figure S18). Overall, hesperidin is capable of binding to the cavity of hACE2 receptor where S protein of the virus interacts, possibly leading to the blocking of virus entry into the host cell.

Molecular dynamics simulations of potential SMs with target protein complex

To check the stability of protein-ligand complex in the real-life environments, we have performed molecular dynamics simulation of selected SM-protein complexes based on docking analysis. For each complex, vacuum minimization, charge neutralization, adding of water solvent (TIP4) and final production run was performed (Gupta, Jadaun, et al., 2015; Gupta, Rao, et al., 2015). The details about the protein-ligand complex behaviour inside systems are explained below:

Epicatechin-Papain like protease complex

We have generated RMSD plot for Epicatechin-Papain like protease trajectories . The figure represents RMSD in protein backbone (blue) and RMSD when ligand is fitted into the cavity of the protein (purple) (Figure S19A). RMSD plot shows that deviation in ligand fitted protein is lower than protein backbone indicating more stability of the complex. Epicatechin-Papain like protease complex deviation gradually increased up to ∼17 ns and then sharp decreased at 20 ns. After this point of time, RMSD further increased exponentially up to ∼24 ns, after which it gradually reduced up to 43 ns. This showed that the complex is reasonably stable during 24–43 ns and well stabilized by end of 50 ns simulation, though a slight increase in the deviation is observed during ∼43.5 to 46.5 ns. RMSF plot was generated to understand atom-based fluctuations in the protein-ligand complex. Positional transitions of amino acids when different forces are applied during 50 ns (Figure S19B). N-terminal 1–20 residues index has fluctuation up to ∼5.8 Å and between 275–285 and 510–520 residues index shows higher fluctuations up to ∼6–7 Å, while the rest of the residues of the protein shows low fluctuations (∼1–3.5Å). Due to these positional amino acid fluctuations, the RMSD of protein is deviating up to ∼7 Å in the initial ∼24 ns. Further, we have investigated behaviour of binding cavity residues in terms of their availability for different type of bonding with epicatechin during the entire simulation. The result indicates that Asp108, Asn109, Gly160, Glu161, Tys264, Asn267, Tyr268, Gln269 and Tyr273 form at least one H-bond and water bridges, while Asp108, Gly160 also form ionic bonds with epicatechin. Tyr273 forms the highest number of H-bonds with Epicatechin followed by Tyr264, Asp108, Tyr268 (Figure S19C). Epicatechin H-bonds with Asp108 and Asn267 and was found in the best pose of the docked complex; these interactions were maintained during the whole simulation. Overall results indicate that epicatechin is capable if inhibiting the papain like protease activity which participates in the cleavage at the N-terminus of the replicase polyprotein of SARS-Cov2.

Epicatechin-Proteinase 3CLPro complex

RMSD plot of epicatechin Proteinase 3CLPro trajectories shows that deviation of protein backbone (blue) is higher than that when the ligand was fitted into the cavity of protein (purple) except at ∼8 to 11.8 ns (Figure 1A). Epicatechin-Proteinase 3CLPro complex deviation gradually increased up to ∼8 ns for Proteinase 3CLPro while in case of the complex it increased up to ∼11.8 ns. After this point of time complex RMSD gradually decreased and got stabilised (RMSD >2.5 Å) till the end of the simulation. RMSF plot of this protein indicates that higher atomic fluctuation was observed in N- and C-terminal residues (∼3.5–4.5 Å) and rest of residues fluctuated in considerable range (∼0.6–2.8 Å) (Figure 1B). Overall, low positional amino acids fluctuation was observed throughout the simulation and this also reflects in low RMSD of the protein. Interaction of binding cavity residues with epicatechin throughout the simulation shows that Thr26, His41, Phe140, Leu141, Ser144, His163, His164, Glu166, Gln189, Thr190, Ala191, Gln192, and Gln306 formed H-bonds and water bridges during the simulation while no residues formed ionic bonds with epicatechin. Glu166, His163 and Gln189 are the major contributors of H-bond formation with epicatechin and are shown, except His163, in the best pose

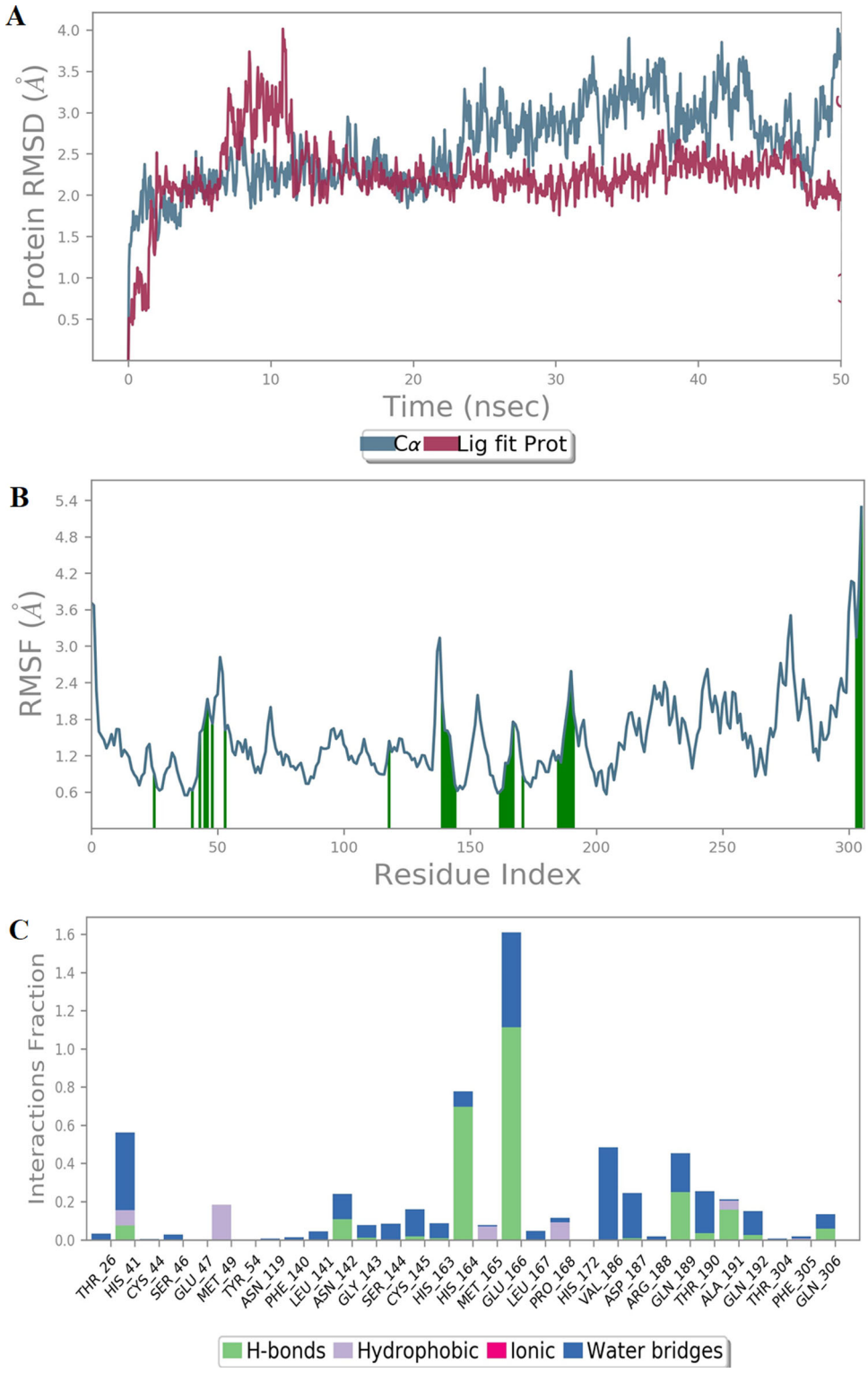

Figure 1. Graphs of (A) RMSD, (B) RMSF plot and (C) different bonds formed by Epicatechin in the cavity of Proteinase 3CLPro during 50 ns.

of docked complex (Figure 1C). This simulation confirms that epicatechin is capable of inhibiting Proteinase 3CLPro.

Epicatechin-RdRp complex

We have generated RMSD plot for epicatechin-RdRp trajectories and it shows that the deviation in protein backbone (blue) is marginally higher than that of the ligand fitted into the cavity of the protein (purple) except at ~0 to 10.5 ns (Figure 2A). A sharp increase in epicatechin-RdRp complex deviation (up to ~ 3 Å) was observed till ~10.5 ns, then this complex obtained stability till end of the simulation. RMSF plot of this protein indicates that higher atomic fluctuations (up to ~5 Å) were observed between 20 and 50 residues of N-terminal and the last 10–15 residues of C-terminal (Figure 2B). Epicatechin forms H-bonds with Ala550, Lys551, Arg555, Tyr619, Ser759, Asp760, Asp761, Ala762, Lys798, Trp800, Glu811, Cys813 and the same residues except Ala762 and Trp800 form water bridges. In

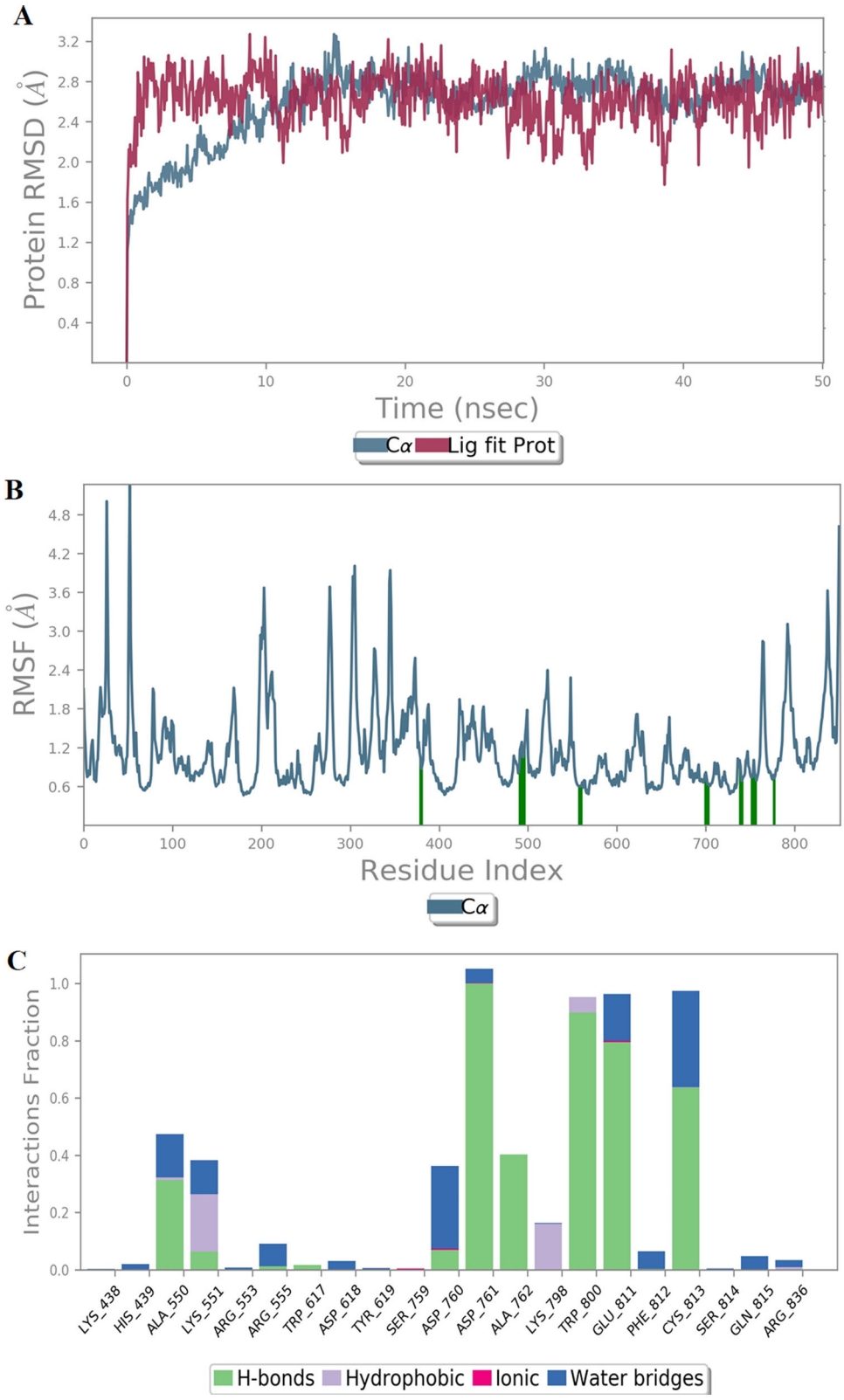

Figure 2. Graphs of (A) RMSD, (B) RMSF plot and (C) different bonds formed by Epicatechin in the cavity of RdRp complex during 50 ns.

addition, Asp760 and Glu811 form ionic bonds with epicatechin (Figure 2C). Asp761, Ala762, Trp800, Glu811, Cys813 residues form higher number of H-bonds with epicatechin which is also found (except Glu811, Cys813 residues) in the best pose of docked complex. These results confirm that epicatechin is a potential inhibitor of RdRp complex.

Epicatechin-NendoU complex

RMSD plot for epicatechin-NendoU trajectories indicates that the deviation in protein backbone (blue) is higher than the protein ligand complex (purple) except between ~2.5 to 3.5 ns (Figure S20A). Epicatechin-NendoU complex deviation is lower than ~ 2.5 Å was observed till end of the simulation

indicated the stable protein ligand infractions. Similarly, RMSF plot of this protein indicates lower atomic fluctuations (>2.0Å) except for few amino acids of N-terminal of C-terminal (Figure S20B). Epicatechin forming H-bond with Lys71, Lys90, Thr196, Ser198, Asn200, Pro271, Met272, Ser274, Thr275 Lys277, Asp297 and forms and water bridges with said residues except Lys71, Thr196, Asp273 (Figure S20C). Similar binding patterns also in the docking complex poses. These simulation results confirm that epicatechin can be a potential inhibitor of NendoU.

Hesperidin-Helicase complex

RMSD plot for hesperidin-Helicase indicates the deviation in protein backbone (blue) is marginally higher than that of the ligand fitted into the cavity of the protein (purple) during whole simulation. Complex deviation falls under the acceptable ranges i.e. ∼3.2 Å (Figure S21A). RMSF plot of this protein indicates that higher atomic fluctuations (up to ∼10.5 Å) was of initial 50 residues of N-terminal of this protein, while remaining residues has fluctuation in acceptable (Figure S21B). During simulation hesperidin forms H-bond with Arg289, Trp292, Gly333, Asp352, Gln354, Leu366, Tyr368, Ser369, Trp385, Asn386, Cys387, Asn422, Lys432 and above residues also forms water bridges except Leu366 (Figure S21C). These results confirm that hesperidin is a potential inhibitor of SARS-CoV-2 helicase.

Hesperidin-Nsp10/Nsp16 complex

RMSD plot for hesperidin-Nsp10/Nsp16 complex (6W75) shows that the deviation in protein backbone (blue) is marginally higher than when the ligand was fitted into the cavity of the protein (purple) throughout the simulation. A sharp increase in deviation (up to ∼ 4.5 Å) was observed till ∼8.8 ns, then this complex attained stability all through the simulation (Figure 3A). RMSF plot of this protein indicates that higher atomic fluctuations ∼4.6 Å and ∼5.5 Å were observed in 285 to 310 residues and 400 to 410 residues of C-terminal respectively (Figure 3B). Hesperidin forms H-bond with Asn6841, Ala6870, Gly6871, Ser6872, Asp6873, Asp6897, Asp6928, Tyr6930, Asp6931, Lys6933, Lys6968, Asn7096 and also form water bridges with same residues except Cys6913 and Phe6947. Additionally, Ala6870, Ser6872, Asp6897 and Asn6899 form ionic bonds with hesperidin (Figure 3C). Gly6871, Asp6897, Cys6913, Asp6928, Asp6931 and Lys6968 residues form H-bonds in the best pose of docked complex and this was retained during the entire simulation. These results confirm that hesperidin is a potential inhibitor of Nsp10/Nsp16 complex.

Hesperidin-hACE2 complex

RMSD plot for Hesperidin-hACE2 complex shows maximum deviation (up to ∼3.2 Å) in protein backbone (blue), is marginally higher than protein-ligand complex backbone (purple) during whole simulation. Protein-ligand deviation was under 2 Å up to ∼45 ns and then a sharp increase (up to ∼3.2 Å) was seen at this point and it keeps reducing till end of the simulation (Figure S22A). RMSF of the protein is under ∼2.5 Å for all residues excepts 120–128 residues (∼2.6 Å and ∼4.5 Å) (Figure S22B). Hesperidin forms H-bond with Gln102, Ala348, Asp350, Asp382, Tyr385, Phe390, Leu391, Arg393, Glu394, Glu398, His401, Lys562 and also forms water bridges with said residues except Phe390. On the other hand, Asp206, Asp350, Asp382, Asn394, Glu398, His401 also form ionic bonds (Figure S22C). H-bonds formed by Gln102, Asp350, Asp382, Tyr385, Leu391, Ala484, Lys562 residues of hACE2 with Hesperidin in the best pose of docked complex are found to be stable throughout the simulation. These simulation results also confirm that hesperidin can work as blocker of virus S protein interaction with hACE2.

Potential multitarget inhibiting SMs as constituents of Anupana

The docking and best pose interaction results indicate that epicatechin, hesperidin, carbazole, murrayanine, murrayaquinone-A, cafestol, embelin and its derivatives are in the top three inhibitors of various functional proteins of SARS-CoV-2 (Table 2). Epicatechin, a flavanol found in tea, apples, red wine, cocoa, raspberry, and pears appears as the most potent inhibitor for multiple targets *viz.* Papain like proteinase, Proteinase 3CLpro, NendoU, RdRp, M and NC proteins of virus (Figure 4). It also showed inhibition efficacy against Nsp6, Nsp7-Nsp8 complex, Nsp9, and ExoN. Hesperidin, a major flavonoid glycoside found in orange, tangerine, lemon, lime, citrus and peppermint showed potential inhibition efficacy for Nsp4, Nsp10-Nsp16 complex, Helicase, ExoN and block the cavity of hACE2 that will possibly protect virus S protein interaction (Figure 5). Embelin and its derivatives found in false black pepper (*Embelia ribes*) showed good inhibition efficacy against Nsp7-Nsp8 complex, Proteinase 3CLPro, Nucleocapsid protein, Nsp1, Nsp2, Nsp10-Nsp16 complex and hACE2. Curry leaf (*Bergera koenigii*) specific carbazole seems to be a potent strong inhibitor for Nsp9, S and M and additionally, its alkaloid derivatives *Viz.* murrayanine, murrayaquinone-A could be a potent inhibitor for Nsp9, S, M and NC. 1-phenylethanethiol, basically responsible for unique sulfury and burnt odour exhibited by curry leaf, is found to be a potent inhibitor for Nsp2. SMs such as aloin, artemisinin, curcumin, withanolide-N found in daily used Indian spices and herbs also showed their prominent inhibition effect in different SARS-CoV2 targets although they showed relatively lower inhibition than epicatechin, hesperidin, carbazole, murrayanine, murrayaquinone-A, cafestol, mangiferin, and embelin. Further, stability of the selected SMs' interaction with targets was confirmed in real time environments by performing MD simulations.

Based on traditional knowledge and results obtained in this study, a preparation of a traditional Ayurvedic formulation Anupana was tested for presence of any of these SMs. HPLC analysis confirmed the presence of epicatechin and hesperidin with retention time of 13.628 and 46.830, respectively (Figure S23). Further, the LC-MS results also confirm the presence of epicatechin, hesperidin and mangiferin in Anupana formulation (Figure S24). We also examined the acute oral toxicity of this Anupana on Wistar rats (OECD Guideline No. 423,

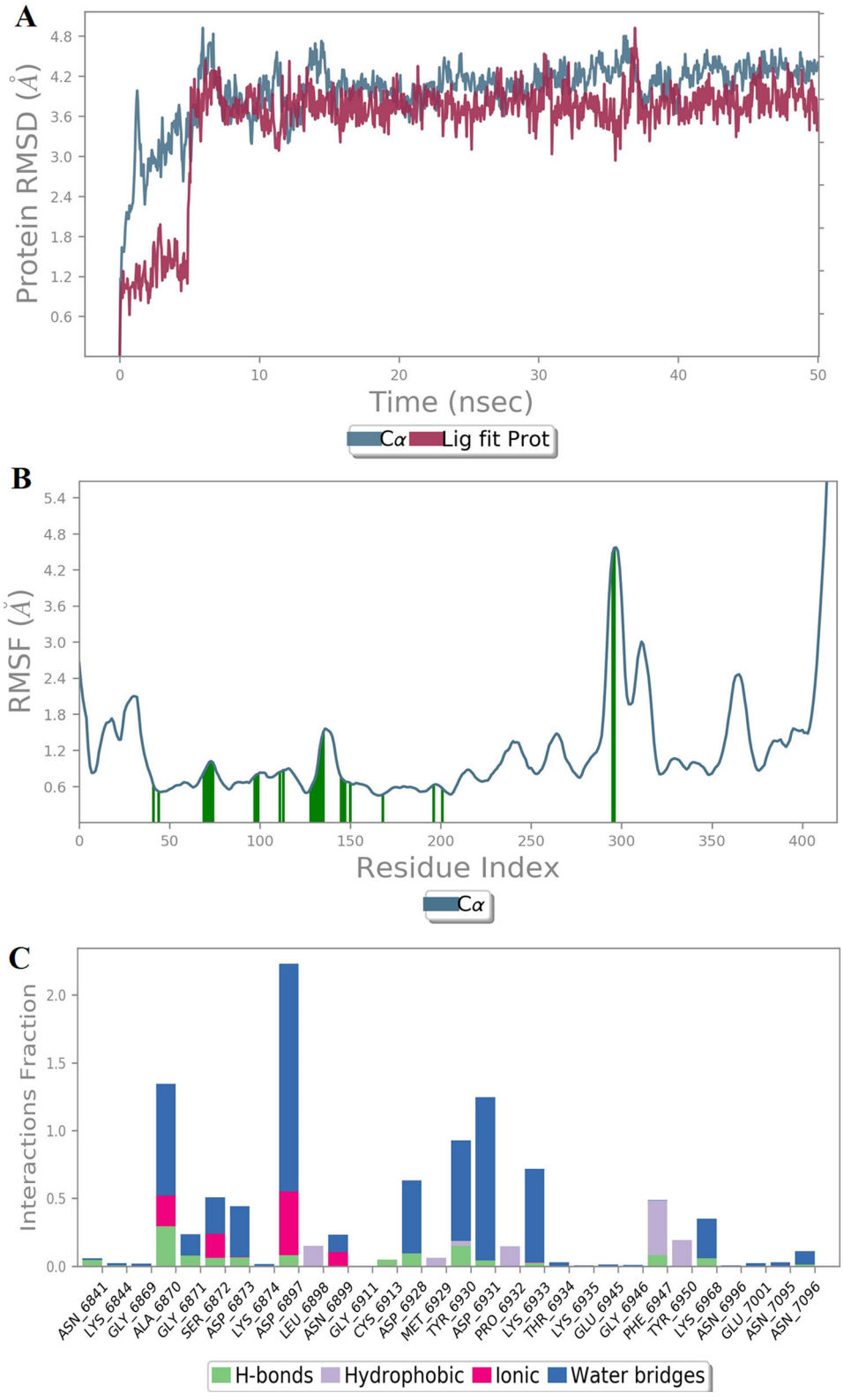

Figure 3. Graphs of (A) RMSD, (B) RMSF plot and (C) different bonds formed by hesperidin in the cavity of Nsp10/NSP16 during 50 ns.

December 2001) and the results showed an LD_{50} >2000 mg/kg body weight and it was classified as category 5 (GHS). The combination of various SMs present in Anupana are well-known antioxidant molecules and are often dubbed as immunity boosters. This study provides molecular basis of antiviral properties of the selected SMs. Since Anupana has been long claimed to be capable of potentiating other drugs, it is fair to expect it to improve the efficacy of drugs used against SARS-CoV-2 viral infection and recovery.

Table 2. List of top 3 inhibitor with their docking score and rank of inhibition efficacy for different targets protein of SARS-Cov-2.

PubChem ID	Proteins/compounds	Nsp1	Nsp2	Papain like proteinase	Nsp4	Proteinase 3CLpro	Nsp6	Nsp7–Nsp8 complex	Nsp9	Nsp10–Nsp16 complex	RdRp	Helicase	ExoN	NendoU	S	M	NC	E	hACE2
									Secondary metabolites										
6854	Carbazole								−6.869*						−5.113*		−4.883†	−4.885*	
96942	Murrayanine																	−4.496†	
127481	Murrayaquinone-A								−6.754$						−4.696$	−5.975†			
141850	1-phenylethanethiol		−5.178$																
129628814	Aloin										−5.547†	−6.305†							
68827	Artemisinin		−5.174†																
969516	Curcumin					−4.298†													
108052	Cafestol			−6.705 †									−7.091†						
53889249	Embelin							−4.678*									−5.192$		
91895880	Embelin-2	−5.555 †								−7.355†									
91895882	Embelin-4					−6.098$	−5.489†												
91895883	Embelin-5											−6.444$							−6.551†
72276	Epicatechin			−7.469*		−6.204*	−5.695$	−4.492$	−5.705†		−5.972*		−7.746$	−5.849*		−6.462*	−5.538*		−6.603$
10621	Hesperidin	−5.769$			−6.822*					−8.17*		−7.132*	−8.358*						−8.111*
5281647	Mangiferin									−7.529$									
23266147	Withanolide-N				−6.716$														
									Known drugs										
3652	Hydroxychloroquine										−5.583$								
404859162	Remdesivir							−4.369†						−5.774†		−6.221$		−4.561$	
37542	Ribavirin	−5.84*					−6.018*							−5.831$	−4.545†				
131411	Arbidol		−7.279*																
6167	Colchicine			−5.293$															
65028	Oseltamivir				−6.54†														

Notes: "*" indicates first best inhibitor; "$" indicates second best inhibitor; "†" indicates third best inhibitor; "Blanks" indicate the respective compound is not found in the top 3 inhibitors among the selected screened compounds for each target protein.

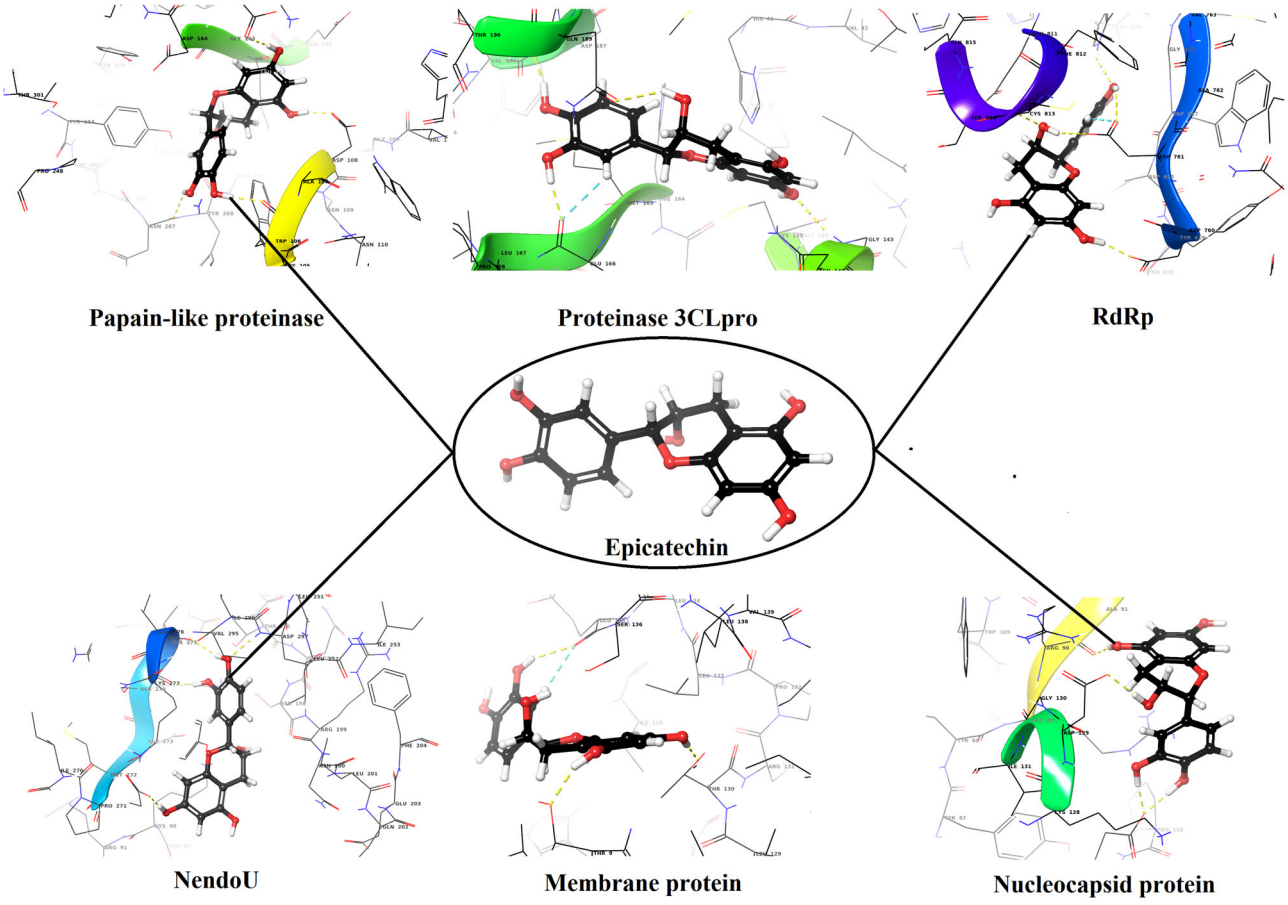

Figure 4. 3D-interaction diagrams of Epicatechin in the cavity of Papain-like proteinase, Proteinase3Clpro, RdRp, NendoU, Membrane and Nucleocapsid protein targets of SARS-CoV-2. Dashed yellow and sky-blue lines indicate H-bonds and electrostatic interactions, respectively.

Discussion

The current COVID-19 pandemic has caused infection to close to 40.4 million people resulting in more than 1.12 million deaths across 213 countries. Further, not a single specific drug has so far been approved for COVID-19 treatment. The re-purposed drug candidates such as Arbidol, Favipiravir, Hydroxychloroquine, Remdesivir, and Ribavirin are reported to elicit varying levels of responses and side effects (Boriskin et al., 2008; Levantovsky & Vabret, 2020; Wang, Cao, Zhang, Liu, et al., 2020; Wang, Cao, Zhang, Yang, et al., 2020; Yao et al., 2020). Most of the treatment strategies involving antivirals are generally single target inhibitors which are not highly effective in combating this virus. Multitarget inhibitors can be potential candidates to address the well-known phenomenon of potential mutations in the virus leading to variants that may escape the treatment regime based on a single target. This prompted us to look for selective herbal and spice SMs and their combinations as potential multitarget inhibitors of SARC-CoV-2. Further, these herbal and spice formulations have been in extensive use in Ayurveda for ages in Asian societies and were found to be safe for human consumption. Many herbs and daily used spices are excellent sources of SMs such as flavonoids, phenylpropanoids, terpenoids, carbazoles and their derivatives having antiviral, anti-inflammatory and antidiabetic properties (Jaseela & Krishna, 2019). The molecular basis of their actions, however, has remained largely unknown.

SARS-CoV-2 possesses a diverse class of proteins and enzymes that are involved in virus RNA replication, suppression of host translation initiation mechanism, transcription, translation, and assembly (Table1). Among them, Papain-like proteinase, Proteinase 3CLpro, RdRp, S and NC are the usual target proteins for the identification of antiviral lead compound identification (Anand et al., 2003; Angeletti et al., 2020; Dai et al., 2020; Gao et al., 2020; Kang et al., 2020; Ou et al., 2020; Romano et al., 2020; Walls et al., 2020). A collection of 69 naturally available SMs from daily used spices and herbs and ten repurposed drugs were screened against multiple protein targets of SARS-CoV-2. Docking and simulation studies revealed that a few SMs, out of 69 tested have better inhibition efficiency against specific protein components of SARS-CoV2 than some of the known drugs (Table 2). Interestingly, our study clearly shows that major functional proteins encoded by the viral genome can potentially be targeted by SMs and therefore, these SMs can likely affect viral life cycle. We showed here that epicatechin, hesperidin, carbazole, murrayanine, murrayaquinone-A, cafestol, mangiferin and embelin show high potential in inhibiting specific SARS-Cov2 proteins. In fact, hesperidin was found to be an efficient protector of hACE2 receptor from attachment by virus S protein. The top five potent inhibitors naturally occur in many herbs and spices i.e. mint, tea, curry leaves, cocoa, citrus, grapes, false black pepper most of which are consumed routinely as part of food. In addition, formulations of these are used for treating

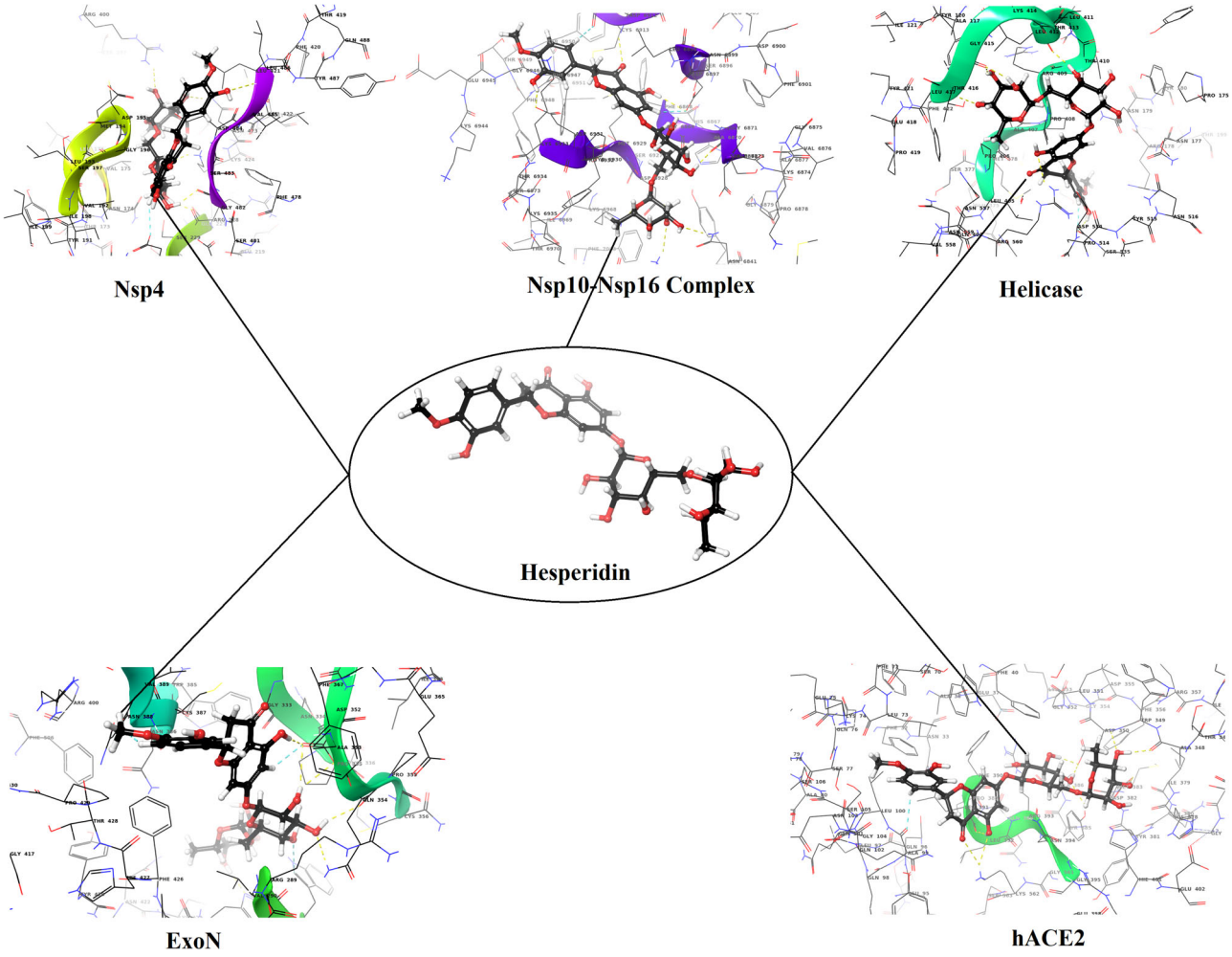

Figure 5. 3D-interaction diagrams of Hesperidin in the cavity of Nsp4, Nsp10-Nsp16 complex, Helicase and ExoN protein targets of SARS-CoV-2 and it also block the virus S protein-interacting domain of hACE2. Dashed yellow and sky-blue lines indicate H-bonds and electrostatic interactions, respectively.

common ailments. Our studies clearly show that one such herbal and spice extract formulation, Anupana contains epicatechin, hesperidin and mangiferin. Epicatechin is also found in tea, apples, red wine, cocoa, raspberry (Natsume et al., 2003; Shay et al., 2015), and pears appears as the most potent inhibitor for multiple targets proteins (Figure 4). It also showed inhibition efficacy against Nsp6, Nsp7-Nsp8 complex, Nsp9, and ExoN. Similarly, hesperidin, a major flavonoid glycoside found in orange, tangerine, lemon, lime, citrus and peppermint (Man et al., 2019) showed potential inhibition efficacy for Nsp4, Nsp10-Nsp16 complex, Helicase, ExoN and block the cavity of hACE2 that will possibly protect virus S protein interaction (Figure 5). Further, stability of the selected SMs-target protein interactions was confirmed in real time environments by performing MD simulations. Some plant SMs are known to exhibit toxicity and preliminary studies on the animal models are required before it is considered safe for human consumption. It is interesting to note that this Anupana is found to be safe as per acute oral toxicity study results. In the absence of inhibitory concentration, clinical data, therapeutic value of these SMs cannot be definitively established. However, the molecular interaction data can be effectively used in developing SMs based preventive nutraceuticals and food supplements.

Conclusion

Computational analysis allowed us to rank the 69 natural spice and herbal SMs and 10 known drugs for their inhibition efficacy against multiple target proteins of SARS-CoV-2 as well as the human ACE2 protein (*in silico*). Epicatechin showed higher inhibition efficacy than Hydroxychloroquine, Remdesivir and Ribavirin against multiple targets i.e. Papain-like proteinase, Proteinase3Clpro, RdRp, NendoU, M and NC while hesperidin showed high inhibition efficiency against Nsp4, Nsp10-Nsp16 complex, Helicase and ExoN of SARS-CoV-2 and S protein-interacting domain of hACE2. Acute oral toxicity studies of Anupana containing the selected SMs epicatechin, hesperidin and mangiferin showed it to be in category 5 (safe for human consumption). The characterized SMs from spices and herbal plant sources may potentially be used in the development of preventive food supplements, nutraceuticals, and antiviral drugs.

Acknowledgements

The authors would like to acknowledge SciGenom Research Foundation (SGRF) for providing financial support to execute this work.

Author contributions

Saurabh Gupta: conceptualization, methodology, data curation, formal analysis, investigation, visualization, supervision, writing—original, and editing. Vishal Singh: docking and dynamics execution, data curation, and visualization. Pritish Kumar Varadwaj: investigation, writing—review and editing, and resources. Navajeet Chakravartty: editing and visualization. A. V. S. Krishna Mohan Katta: writing—review and editing, and visualization. Sivarama Prasad Lekkala: writing—review and editing. George Thomas: conceptualization, writing—review and editing, and funding acquisition. Srinivasan Narasimhan: validation, conceptualization, and writing—review and editing. Arjula R. Reddy: supervision and writing—review and editing. V. B. Reddy Lachagari: supervision, conceptualization, project administration, and funding acquisition. All authors agree to be accountable for all aspects of work ensuring integrity and accuracy.

Disclosure statement

All authors declare that they have no conflict of interest. S. N. has developed an Anupana formulation that is being improvised based on the results reported here and has filed a patent application at Intellectual Property India with reference no. 202041028177.

ORCID

Saurabh Gupta http://orcid.org/0000-0002-1327-7389
Pritish Kumar Varadwaj http://orcid.org/0000-0001-5706-2411
Navajeet Chakravartty http://orcid.org/0000-0002-0663-0113
Sivarama Prasad Lekkala http://orcid.org/0000-0002-4973-0659
George Thomas http://orcid.org/0000-0003-1914-5923
V. B. Reddy Lachagari http://orcid.org/0000-0002-4708-7866

References

Almeida, M. S., Johnson, M. A., Herrmann, T., Geralt, M., & Wüthrich, K. (2007). Novel beta-barrel fold in the nuclear magnetic resonance structure of the replicase nonstructural protein 1 from the severe acute respiratory syndrome coronavirus. *Journal of Virology*, *81*(7), 3151–3161. https://doi.org/10.1128/JVI.01939-06

Anand, K., Ziebuhr, J., Wadhwani, P., Mesters, J. R., & Hilgenfeld, R. (2003). Coronavirus main proteinase (3CLpro) structure: Basis for design of anti-SARS drugs. *Science (New York, N.Y.)*, *300*(5626), 1763–1767. https://doi.org/10.1126/science.1085658

Ang, L., Lee, H. W., Choi, J. Y., Zhang, J., & Lee, M. S. (2020). Herbal medicine and pattern identification for treating COVID-19: A rapid review of guidelines. *Integrative Medicine Research*, *9*(2), 100407. https://doi.org/10.1016/j.imr.2020.100407

Angeletti, S., Benvenuto, D., Bianchi, M., Giovanetti, M., Pascarella, S., & Ciccozzi, M. (2020). COVID-2019: The role of the nsp2 and nsp3 in its pathogenesis. *Journal of Medical Virology*, *92*(6), 584–588. https://doi.org/10.1002/jmv.25719

Astuti, I., & Ysrafil. (2020). Severe acute respiratory syndrome coronavirus 2 (SARS-CoV-2): An overview of viral structure and host response. *Diabetes & Metabolic Syndrome: Clinical Research & Reviews*, *14*(4), 407–412. https://doi.org/10.1016/j.dsx.2020.04.020

Benvenuto, D., Angeletti, S., Giovanetti, M., Bianchi, M., Pascarella, S., Cauda, R., Ciccozzi, M., & Cassone, A. (2020). Evolutionary analysis of SARS-CoV-2: How mutation of non-structural protein 6 (NSP6) could affect viral autophagy. *Journal of Infection*, *81*(1), e24–e27. https://doi.org/10.1016/j.jinf.2020.03.058

Bianchi, M., Benvenuto, D., Giovanetti, M., Angeletti, S., Ciccozzi, M., & Pascarella, S. (2020). Sars CoV-2 Envelope and Membrane proteins: Differences from closely related proteins linked to cross-species transmission? *BioMed Research International*, *2020*, 4389089.

Boriskin, Y. S., Leneva, I. A., Pecheur, E. I., & Polyak, S. J. (2008). Arbidol: A broad-spectrum antiviral compound that blocks viral fusion. *Current Medicinal Chemistry*, *15*(10), 997–1005. https://doi.org/10.2174/092986708784049658

Bowers, K. J., Chow, D. E., Xu, H., Dror, R. O., Eastwood, M. P., Gregersen, B. A., … Salmon, J. K. (2006). Scalable algorithms for molecular dynamics simulations on commodity clusters. In *SC'06: Proceedings of the 2006 ACM/IEEE Conference on Supercomputing* (pp. 43–43). IEEE.

Chowdhury, R., & Maranas, C. D. (2020). Biophysical characterization of the SARS-CoV2 spike protein binding with the ACE2 receptor explains increased COVID-19 pathogenesis. *BioRxiv*. https://doi.org/10.1101/2020.03.30.015891

Covey, T. R., Lee, E. D., Bruins, A. P., & Henion, J. D. (1986). Liquid chromatography/mass spectrometry. *Analytical Chemistry*, *58*(14), 1451A–1461A. https://doi.org/10.1021/ac00127a001

Dai, W., Zhang, B., Jiang, X.-M., Su, H., Li, J., Zhao, Y., Xie, X., Jin, Z., Peng, J., Liu, F., Li, C., Li, Y., Bai, F., Wang, H., Cheng, X., Cen, X., Hu, S., Yang, X., Wang, J., … Liu, H. (2020). Structure-based design of antiviral drug candidates targeting the SARS-CoV-2 main protease. *Science (New York, N.Y.)*, *368*(6497), 1331–1335. https://doi.org/10.1126/science.abb4489

Decroly, E., Debarnot, C., Ferron, F., Bouvet, M., Coutard, B., Imbert, I., Gluais, L., Papageorgiou, N., Sharff, A., Bricogne, G., Ortiz-Lombardia, M., Lescar, J., & Canard, B. (2011). Crystal structure and functional analysis of the SARS-coronavirus RNA cap 2′-O-methyltransferase nsp10/nsp16 complex. *PLoS Pathogens*, *7*(5), e1002059. https://doi.org/10.1371/journal.ppat.1002059

Dong, S., Sun, J., Mao, Z., Wang, L., Lu, Y. L., & Li, J. (2020). A guideline for homology modeling of the proteins from newly discovered betacoronavirus, 2019 novel coronavirus (2019-nCoV). *Journal of Medical Virology*, *92*(9), 1542–1548. https://doi.org/10.1002/jmv.25768

Drosten, C., Günther, S., Preiser, W., van der Werf, S., Brodt, H.-R., Becker, S., Rabenau, H., Panning, M., Kolesnikova, L., Fouchier, R. A. M., Berger, A., Burguière, A.-M., Cinatl, J., Eickmann, M., Escriou, N., Grywna, K., Kramme, S., Manuguerra, J.-C., Müller, S., … Doerr, H. W. (2003). Identification of a novel coronavirus in patients with severe acute respiratory syndrome. *The New England Journal of Medicine*, *348*(20), 1967–1976. https://doi.org/10.1056/NEJMoa030747

Dutta, K., Shityakov, S., Morozova, O., Khalifa, I., Zhang, J., Panda, A., & Ghosh, C. (2020). Beclabuvir can inhibit the RNA-dependent RNA polymerase of newly emerged novel coronavirus (SARS-CoV-2). *Preprints*. https://doi.org/10.20944/preprints202003.0395.v2

Ferron, F., Subissi, L., Silveira De Morais, A. T., Le, N. T. T., Sevajol, M., Gluais, L., Decroly, E., Vonrhein, C., Bricogne, G., Canard, B., & Imbert, I. (2018). Structural and molecular basis of mismatch correction and ribavirin excision from coronavirus RNA. *Proceedings of the National Academy of Sciences of the United States of America*, *115*(2), E162–E171. https://doi.org/10.1073/pnas.1718806115

Gao, Y., Yan, L., Huang, Y., Liu, F., Zhao, Y., Cao, L., Wang, T., Sun, Q., Ming, Z., Zhang, L., Ge, J., Zheng, L., Zhang, Y., Wang, H., Zhu, Y., Zhu, C., Hu, T., Hua, T., Zhang, B., … Rao, Z. (2020). Structure of the RNA-dependent RNA polymerase from COVID-19 virus. *Science (New York, N.Y.)*, *368*(6492), 779–782. https://doi.org/10.1126/science.abb7498

Ge, X.-Y., Li, J.-L., Yang, X.-L., Chmura, A. A., Zhu, G., Epstein, J. H., Mazet, J. K., Hu, B., Zhang, W., Peng, C., Zhang, Y.-J., Luo, C.-M., Tan, B., Wang, N., Zhu, Y., Crameri, G., Zhang, S.-Y., Wang, L.-F., Daszak, P., & Shi, Z.-L. (2013). Isolation and characterization of a bat SARS-like coronavirus that uses the ACE2 receptor. *Nature*, *503*(7477), 535–538. https://doi.org/10.1038/nature12711

Guan, W.-J., Ni, Z.-Y., Hu, Y., Liang, W.-H., Ou, C.-Q., He, J.-X., Liu, L., Shan, H., Lei, C.-L., Hui, D. S. C., Du, B., Li, L.-J., Zeng, G., Yuen, K.-Y., Chen, R.-C., Tang, C.-L., Wang, T., Chen, P.-Y., Xiang, J., … Zhong, N.-S. (2020). Clinical characteristics of coronavirus disease 2019 in China. *The New England Journal of Medicine*, *382*(18), 1708–1720. https://doi.org/10.1056/NEJMoa2002032

Gupta, S., Jadaun, A., Kumar, H., Raj, U., Varadwaj, P. K., & Rao, A. R. (2015). Exploration of new drug-like inhibitors for serine/threonine protein phosphatase 5 of Plasmodium falciparum: A docking and simulation study. *Journal of Biomolecular Structure & Dynamics*, *33*(11), 2421–2441. https://doi.org/10.1080/07391102.2015.1051114

Gupta, S., Rao, A. R., Varadwaj, P. K., De, S., & Mohapatra, T. (2015). Extrapolation of inter domain communications and substrate binding cavity of camel HSP70 1A: A molecular modeling and dynamics simulation study. *PLoS One*, *10*(8), e0136630. https://doi.org/10.1371/journal.pone.0136630

Hao, W., Wojdyla, J. A., Zhao, R., Han, R., Das, R., Zlatev, I., Manoharan, M., Wang, M., & Cui, S. (2017). Crystal structure of Middle East respiratory syndrome coronavirus helicase. *PLoS Pathogens*, *13*(6), e1006474. https://doi.org/10.1371/journal.ppat.1006474

Huang, C., Wang, Y., Li, X., Ren, L., Zhao, J., Hu, Y., Zhang, L., Fan, G., Xu, J., Gu, X., Cheng, Z., Yu, T., Xia, J., Wei, Y., Wu, W., Xie, X., Yin, W., Li, H., Liu, M., … Cao, B. (2020). Clinical features of patients infected with 2019 novel coronavirus in Wuhan, China. *The Lancet*, *395*(10223), 497–506. https://doi.org/10.1016/S0140-6736(20)30183-5

Jaseela, V. K., & Krishna, J. G. (2019). Anupana—A critical review. *Journal of Ayurveda and Integrated Medical Sciences*, *4*(5), 311–317.

Jauregui, A. R., Savalia, D., Lowry, V. K., Farrell, C. M., & Wathelet, M. G. (2013). Identification of residues of SARS-CoV nsp1 that differentially affect inhibition of gene expression and antiviral signaling. *PLoS One*, *8*(4), e62416. https://doi.org/10.1371/journal.pone.0062416

Jia, Z., Yan, L., Ren, Z., Wu, L., Wang, J., Guo, J., Zheng, L., Ming, Z., Zhang, L., Lou, Z., & Rao, Z. (2019). Delicate structural coordination of the severe acute respiratory syndrome coronavirus Nsp13 upon ATP hydrolysis. *Nucleic Acids Research*, *47*(12), 6538–6550. https://doi.org/10.1093/nar/gkz409

Kim, Y., Jedrzejczak, R., Maltseva, N. I., Wilamowski, M., Endres, M., Godzik, A., Michalska, K., & Joachimiak, A. (2020). Crystal structure of Nsp15 endoribonuclease NendoU from SARS-CoV-2. *Protein Science*, *29*(7), 1596–1605. https://doi.org/10.1002/pro.3873

Kang, S., Yang, M., Hong, Z., Zhang, L., Huang, Z., Chen, X., He, S., Zhou, Z., Zhou, Z., Chen, Q. & Yan, Y. (2020). Crystal structure of SARS-CoV-2 nucleocapsid protein RNA binding domain reveals potential unique drug targeting sites. *Acta Pharmaceutica Sinica B*.

Kirchdoerfer, R. N., Wang, N., Pallesen, J., Wrapp, D., Turner, H. L., Cottrell, C. A., Corbett, K. S., Graham, B. S., McLellan, J. S., & Ward, A. B. (2018). Stabilized coronavirus spikes are resistant to conformational changes induced by receptor recognition or proteolysis. *Scientific Reports*, *8*(1), 1–11. https://doi.org/10.1038/s41598-018-36918-8

Ksiazek, T. G., Erdman, D., Goldsmith, C. S., Zaki, S. R., Peret, T., Emery, S., Tong, S., Urbani, C., Comer, J. A., Lim, W., Rollin, P. E., Dowell, S. F., Ling, A.-E., Humphrey, C. D., Shieh, W.-J., Guarner, J., Paddock, C. D., Rota, P., Fields, B., … Anderson, L. J. (2003). A novel coronavirus associated with severe acute respiratory syndrome. *The New England Journal of Medicine*, *348*(20), 1953–1966. https://doi.org/10.1056/NEJMoa030781

Levantovsky, R., & Vabret, N. (2020). Hydroxychloroquine: small effects in mild disease. *Nat Rev Immunol*, *20*, 350. https://doi.org/10.1038/s41577-020-0315-4

Littler, D., Gully, B., Colson, R. N., & Rossjohn, J. (2020). Crystal structure of the SARS-CoV-2 non-structural protein 9, Nsp9. *iScience*, *23*(7), 101258.

Lokugamage, K. G., Narayanan, K., Huang, C., & Makino, S. (2012). Severe acute respiratory syndrome coronavirus protein nsp1 is a novel eukaryotic translation inhibitor that represses multiple steps of translation initiation. *Journal of Virology*, *86*(24), 13598–13608. https://doi.org/10.1128/JVI.01958-12

Ma, Y., Wu, L., Shaw, N., Gao, Y., Wang, J., Sun, Y., Lou, Z., Yan, L., Zhang, R., & Rao, Z. (2015). Structural basis and functional analysis of the SARS coronavirus nsp14-nsp10 complex. *Proceedings of the National Academy of Sciences of the United States of America*, *112*(30), 9436–9441. https://doi.org/10.1073/pnas.1508686112

Man, M. Q., Yang, B., & Elias, P. M. (2019). Benefits of hesperidin for cutaneous functions. *Evidence-Based Complementary and Alternative Medicine*, *2019*, 2676307.

Natsume, M., Osakabe, N., Oyama, M., Sasaki, M., Baba, S., Nakamura, Y., Osawa, T., & Terao, J. (2003). Structures of (−)-epicatechin glucuronide identified from plasma and urine after oral ingestion of (−)-epicatechin: Differences between human and rat. *Free Radical Biology & Medicine*, *34*(7), 840–849. https://doi.org/10.1016/S0891-5849(02)01434-X

Ou, X., Liu, Y., Lei, X., Li, P., Mi, D., Ren, L., Guo, L., Guo, R., Chen, T., Hu, J., Xiang, Z., Mu, Z., Chen, X., Chen, J., Hu, K., Jin, Q., Wang, J., & Qian, Z. (2020). Characterization of spike glycoprotein of SARS-CoV-2 on virus entry and its immune cross-reactivity with SARS-CoV. *Nature Communications*, *11*(1), 1–12. https://doi.org/10.1038/s41467-020-15562-9

Owusu, M., Annan, A., Corman, V. M., Larbi, R., Anti, P., Drexler, J. F., Agbenyega, O., Adu-Sarkodie, Y., & Drosten, C. (2014). Human coronaviruses associated with upper respiratory tract infections in three rural areas of Ghana. *PloS One*, *9*(7), e99782. https://doi.org/10.1371/journal.pone.0099782

Romano, M., Ruggiero, A., Squeglia, F., Maga, G., & Berisio, R. (2020). A structural view at SARS-CoV-2 RNA replication machinery: RNA synthesis, proofreading and final capping. *Cells*, *9*(5), 1267.

Sachan, A. K., Kumar, S., Kumari, K., & Singh, D. (2018). Medicinal uses of spices used in our traditional culture: Worldwide. *Journal of Medicinal Plants Studies*, *6*(3), 116–122.

Sakai, Y., Kawachi, K., Terada, Y., Omori, H., Matsuura, Y., & Kamitani, W. (2017). Two-amino acids change in the nsp4 of SARS coronavirus abolishes viral replication. *Virology*, *510*, 165–174. https://doi.org/10.1016/j.virol.2017.07.019

Sakakibara, H., Honda, Y., Nakagawa, S., Ashida, H., & Kanazawa, K. (2003). Simultaneous determination of all polyphenols in vegetables, fruits, and teas. *Journal of Agricultural and Food Chemistry*, *51*(3), 571–581. https://doi.org/10.1021/jf020926l

Sanders, J. M., Monogue, M. L., Jodlowski, T. Z., & Cutrell, J. B. (2020). Pharmacologic treatments for coronavirus disease 2019 (COVID-19): A review. *JAMA*, *323*(18), 1824–1836.

Schoeman, D., & Fielding, B. C. (2019). Coronavirus envelope protein: Current knowledge. *Virology Journal*, *16*(1), 69. https://doi.org/10.1186/s12985-019-1182-0

Shay, J., Elbaz, H. A., Lee, I., Zielske, S. P., Malek, M. H., & Hüttemann, M. (2015). Molecular mechanisms and therapeutic effects of (−)-epicatechin and other polyphenols in cancer, inflammation, diabetes, and neurodegeneration. *Oxidative Medicine and Cellular Longevity*, *2015*, 181260. https://doi.org/10.1155/2015/181260

Shen, Z., Wang, G., Yang, Y., Shi, J., Fang, L., Li, F., Xiao, S., Fu, Z. F., & Peng, G. (2019). A conserved region of nonstructural protein 1 from alphacoronaviruses inhibits host gene expression and is critical for viral virulence. *The Journal of Biological Chemistry*, *294*(37), 13606–13618. https://doi.org/10.1074/jbc.RA119.009713

Shereen, M. A., Khan, S., Kazmi, A., Bashir, N., & Siddique, R. (2020). COVID-19 infection: Origin, transmission, and characteristics of human coronaviruses. *Journal of Advanced Research*, *24*, 91–98. https://doi.org/10.1016/j.jare.2020.03.005

Song, W., Gui, M., Wang, X., & Xiang, Y. (2018). Cryo-EM structure of the SARS coronavirus spike glycoprotein in complex with its host cell receptor ACE2. *PLoS Pathogens*, *14*(8), e1007236. https://doi.org/10.1371/journal.ppat.1007236

Sutton, G., Fry, E., Carter, L., Sainsbury, S., Walter, T., Nettleship, J., Berrow, N., Owens, R., Gilbert, R., Davidson, A., Siddell, S., Poon, L. L. M., Diprose, J., Alderton, D., Walsh, M., Grimes, J. M., & Stuart, D. I. (2004). The nsp9 replicase protein of SARS-coronavirus, structure and functional insights. *Structure*, *12*(2), 341–353. https://doi.org/10.1016/j.str.2004.01.016

Te Velthuis, A. J., van den Worm, S. H., & Snijder, E. J. (2012). The SARS-coronavirus nsp7 + nsp8 complex is a unique multimeric RNA polymerase capable of both de novo initiation and primer extension. *Nucleic Acids Research*, *40*(4), 1737–1747. https://doi.org/10.1093/nar/gkr893

Walls, A. C., Park, Y. J., Tortorici, M. A., Wall, A., McGuire, A. T., & Veesler, D. (2020). Structure, function, and antigenicity of the SARS-CoV-2 spike glycoprotein. *Cell*, *181*(2), 281–292.e6. https://doi.org/10.1016/j.cell.2020.02.058

Wan, Y., Shang, J., Graham, R., Baric, R. S., & Li, F. (2020). Receptor recognition by the novel coronavirus from Wuhan: An analysis based on decade-long structural studies of SARS coronavirus. *Journal of Virology*, *94*(7), e00127-20. https://doi.org/10.1128/JVI.00127-20

Wang, W., Xu, Y., Gao, R., Lu, R., Han, K., Wu, G., & Tan, W. (2020). Detection of SARS-CoV-2 in different types of clinical specimens. *JAMA*, *323*(18), 1843–1844.

Wang, X., Cao, R., Zhang, H., Liu, J., Xu, M., Hu, H., Li, Y., Zhao, L., Li, W., Sun, X., Yang, X., Shi, Z., Deng, F., Hu, Z., Zhong, W., & Wang, M. (2020). The anti-influenza virus drug, arbidol is an efficient inhibitor of SARS-CoV-2 in vitro. *Cell Discovery*, *6*(1), 1–5. https://doi.org/10.1038/s41421-020-0169-8

Wang, M., Cao, R., Zhang, L., Yang, X., Liu, J., Xu, M., Shi, Z., Hu, Z., Zhong, W., & Xiao, G. (2020). Remdesivir and chloroquine effectively inhibit the recently emerged novel coronavirus (2019-nCoV) in vitro. *Cell Research*, *30*(3), 269–271. https://doi.org/10.1038/s41422-020-0282-0

Wang, M., Yan, M., Xu, H., Liang, W., Kan, B., Zheng, B., Chen, H., Zheng, H., Xu, Y., Zhang, E., Wang, H., Ye, J., Li, G., Li, M., Cui, Z., Liu, Y.-F.,

Guo, R.-T., Liu, X.-N., Zhan, L.-H., … Xu, J. (2005). SARS-CoV infection in a restaurant from palm civet. *Emerging Infectious Diseases*, *11*(12), 1860–1865. https://doi.org/10.3201/eid1112.041293

Wu, C., Liu, Y., Yang, Y., Zhang, P., Zhong, W., Wang, Y., Wang, Q., Xu, Y., Li, M., Li, X., Zheng, M., Chen, L., & Li, H. (2020). Analysis of therapeutic targets for SARS-CoV-2 and discovery of potential drugs by computational methods. *Acta Pharmaceutica Sinica. B*, *10*(5), 766–788. https://doi.org/10.1016/j.apsb.2020.02.008

Wu, F., Zhao, S., Yu, B., Chen, Y.-M., Wang, W., Song, Z.-G., Hu, Y., Tao, Z.-W., Tian, J.-H., Pei, Y.-Y., Yuan, M.-L., Zhang, Y.-L., Dai, F.-H., Liu, Y., Wang, Q.-M., Zheng, J.-J., Xu, L., Holmes, E. C., & Zhang, Y.-Z. (2020). A new coronavirus associated with human respiratory disease in China. *Nature*, *579*(7798), 265–269. https://doi.org/10.1038/s41586-020-2008-3

Yao, X., Ye, F., Zhang, M., Cui, C., Huang, B., Niu, P., Liu, X., Zhao, L., Dong, E., Song, C., Zhan, S., Lu, R., Li, H., Tan, W., & Liu, D. (2020). In vitro antiviral activity and projection of optimized dosing design of hydroxychloroquine for the treatment of severe acute respiratory syndrome coronavirus 2 (SARS-CoV-2). *Clinical Infectious Diseases*, *71*(15), 732–739. https://doi.org/10.1093/cid/ciaa237

Zachariah, T. J., & Leela, N. K. (2018). Spices: Secondary metabolites and medicinal properties. In *Indian spices* (pp. 277–316). Springer.

Zaki, A. M., Van Boheemen, S., Bestebroer, T. M., Osterhaus, A. D., & Fouchier, R. A. (2012). Isolation of a novel coronavirus from a man with pneumonia in Saudi Arabia. *The New England Journal of Medicine*, *367*(19), 1814–1820. https://doi.org/10.1056/NEJMoa1211721

Zhou, P., Yang, X.-L., Wang, X.-G., Hu, B., Zhang, L., Zhang, W., Si, H.-R., Zhu, Y., Li, B., Huang, C.-L., Chen, H.-D., Chen, J., Luo, Y., Guo, H., Jiang, R.-D., Liu, M.-Q., Chen, Y., Shen, X.-R., Wang, X., … Shi, Z.-L. (2020). A pneumonia outbreak associated with a new coronavirus of probable bat origin. *Nature*, *579*(7798), 270–273. https://doi.org/10.1038/s41586-020-2012-7

Zhu, N., Zhang, D., Wang, W., Li, X., Yang, B., Song, J., Zhao, X., Huang, B., Shi, W., Lu, R., Niu, P., Zhan, F., Ma, X., Wang, D., Xu, W., Wu, G., Gao, G. F., & Tan, W. (2020). A novel coronavirus from patients with pneumonia in China, 2019. *The New England Journal of Medicine*, *382*(8), 727–733. https://doi.org/10.1056/NEJMoa2001017